

A study of dissipative models based on Dirac matrices

Jyotsna Gidugu^{1,*} and Daniel P. Arovas^{1,†}

¹*Department of Physics, University of California San Diego, La Jolla, CA 92093, USA*

(Dated: September 11, 2023)

We generalize the recent work of Shibata and Katsura [1], who considered a $S = \frac{1}{2}$ chain with alternating XX and YY couplings in the presence of dephasing, the dynamics of which are described by the GKLS master equation. Their model is equivalent to a non-Hermitian system described by the Kitaev formulation [2] in terms of a single Majorana species hopping on a two-leg ladder in the presence of a nondynamical \mathbb{Z}_2 gauge field. Our generalization involves Dirac gamma matrix ‘spin’ operators on the square lattice, and maps onto a non-Hermitian square lattice bilayer which is also Kitaev-solvable. We describe the exponentially many non-equilibrium steady states in this model. We identify how the spin degrees of freedom can be accounted for in the 2d model in terms of the gauge-invariant quantities and then proceed to study the Liouvillian spectrum. We use a genetic algorithm to estimate the Liouvillian gap and the first decay modes for large system sizes. We observe a transition in the first decay modes, similar to that in ref. [1]. The results we obtain are consistent with a perturbative analysis for small and large values of the dissipation strength.

I. INTRODUCTION

Open quantum systems afford us the opportunity to study phenomena such as relaxational quantum dynamics for systems coupled to a bath [3]. Typically this involves ‘integrating out’ or eliminating in some way the bath degrees of freedom, resulting in a dynamics for the system itself in terms of its reduced density matrix: $\dot{\rho} = \mathcal{L}\rho$, where \mathcal{L} is the Liouvillian operator. At long times, the system relaxes to a non-equilibrium steady state (NESS); the existence of a NESS is guaranteed by the dynamics, but under special circumstances owing to, for example, extra conserved quantities, the NESS may not be unique.

For noninteracting systems, hybridization with the bath degrees of freedom still results in a solvable (quadratic) model [4]. For interacting systems, solvable models are rare, and numerical approaches are challenging. This is especially true for density matrix evolution since one must keep track of not just populations $|\alpha\rangle\langle\alpha|$ but also the coherences $|\alpha\rangle\langle\beta|$ with $\alpha \neq \beta$, effectively squaring the size of the problem *vis-a-vis* the system’s Hilbert space dimension.

Recently, Shibata and Katsura [1] (SK) described a model of open system dynamics based on the GKLS master equation [5] which, though interacting, is solvable in the sense of Kitaev’s celebrated honeycomb lattice Hamiltonian model [2]. That is to say, the evolution of $\rho(t)$ under the Liouvillian \mathcal{L} is effectively described by a non-interacting dynamics in the presence of a static \mathbb{Z}_2 gauge field. While in each gauge sector the evolution is described by a quadratic, albeit non-Hermitian, Hamiltonian, there are exponentially many gauge sectors to evaluate (which in general have no discrete space group symmetries), and in this sense the general problem is intractable. For the Hermitian Kitaev model, oftentimes

the ground state may be ascertained with help from a remarkable theorem by Lieb [6], which provides valuable information regarding much of the gauge-invariant content of the ground state, *i.e.* the \mathbb{Z}_2 plaquette fluxes. For the non-Hermitian case, however, we know of no generalization of Lieb’s theorem which constrains the gauge-invariant content of, say, the longest-lived decaying density matrix. Thus, in general one must resort to numerics if one is interested in the complex spectrum of \mathcal{L} .

The Shibata-Katsura construction involves a $S = \frac{1}{2}$ chain where each site is coupled to an environmental bath. Within the GKLS formalism, this results in an effective two leg ladder system, where one leg corresponds to the bra states and the other to the ket states of the density matrix, and the rungs of the ladder contribute non-Hermitian terms which result from the effective elimination of the bath degrees of freedom. The ladder is thus three-fold coordinated, and the model is constructed so that it satisfies the Kitaev solvability criteria §II C). Our main goal is to introduce and analyze a generalization of the SK model to two space dimensions, based on a 4×4 gamma matrix generalization of the Hamiltonian Kitaev model [7, 8]. As the dissipative SK model is described by non-Hermitian Hamiltonian evolution on the ladder, our model is described by such an evolution on a square lattice bilayer. As we shall see, while our model is a direct analog of SK in some sense, it also entails some important differences – in particular, an extensive number of conserved quantities leading to exponentially many NESSes.

We first discuss various preliminaries, including the GKLS master equation, its vectorization and description in terms of non-Hermitian Hamiltonian evolution on a product Hilbert space, the Shibata-Katsura model, gamma matrix generalizations of the Kitaev honeycomb model, and finally our extension of SK to a dissipative square lattice model involving 4×4 Dirac matrix ‘spin’ operators.

Note: While this paper was in the final stages of preparation, two analyses of a largely equivalent model ap-

* jgidugu@ucsd.edu

† darovas@ucsd.edu

peared on the arXiv [9, 10].

II. PRELIMINARIES

A. The GKLS master equation

An open quantum system S is one which unitarily co-evolves with an environment E under a Hamiltonian $H = H_S + H_E + H_{\text{int}}$, where H_{int} couples S and E . The expectation of any operator \mathcal{O} restricted to S is given by $\langle \mathcal{O}(t) \rangle = \text{Tr}(\varrho_S(t) \mathcal{O})$, where $\varrho_S(t)$ is the time-dependent reduced density matrix of S , *i.e.* $\varrho_S(t) = \text{Tr}_E \varrho_U(t)$, where $\varrho_U(t)$ is the full density matrix describing the ‘universe’ $U = S \cup E$. Under certain assumptions, the dynamics of the system’s reduced density matrix is described by the GKLS master equation [3, 5],

$$\frac{d\varrho}{dt} = -i[H, \varrho] + \sum_a \left(L_a \varrho L_a^\dagger - \frac{1}{2} L_a^\dagger L_a \varrho - \frac{1}{2} \varrho L_a^\dagger L_a \right), \quad (1)$$

Here and henceforth we drop the subscript S on ϱ_S . The $\{L_a\}$ are the Lindblad jump operators, which describe the effects of the system-environment coupling on ϱ after the environment is traced out. H is the ‘Lamb shift Hamiltonian’, which commutes with H_S and includes renormalizations of the system’s unperturbed energy levels resulting from the environmental couplings. In the absence of all such couplings, we recover the usual Liouville evolution $\dot{\varrho} = -i[H_S, \varrho]$.

The full GKLS evolution in eqn. 1 is of the form $\dot{\varrho} = \mathcal{L}\varrho$. Assuming \mathcal{L} is time-independent, one may formally write $\varrho(t) = \exp(\mathcal{L}t)\varrho(0)$, which defines for each t a map $\Phi_t: \varrho(0) \mapsto \varrho(t)$ which possesses the following salient properties: (i) linearity, (ii) trace-preserving, (iii) Hermiticity preserving, and (iv) complete positivity [3]. Writing $\varrho(t) = \sum_{j,k} \varrho_{jk}(t) |j\rangle\langle k|$ in terms of basis states, we may write $\dot{\varrho}_{jk} = \mathcal{L}_{jk,lm} \varrho_{lm}$, where $\mathcal{L}_{jk,lm}$ is a supermatrix of dimension N^2 , where N is the dimension of the basis and $(jk)/(lm)$ are composite indices. Generically \mathcal{L} is not a normal matrix, *i.e.* $[\mathcal{L}, \mathcal{L}^\dagger] \neq 0$, and its eigenvalues Λ_a may be complex. However, since the evolution is trace-preserving, one has that δ_{jk} is a left-eigenvector of \mathcal{L} with eigenvalue zero. The corresponding right eigenvector is the NESS, $\varrho_{lm}^{\text{NESS}}$. Under special circumstances there may be more than one NESS [11]. Positivity entails that $\text{Re} \Lambda_a \leq 0$ for each eigenvalue of the Liouvillian \mathcal{L} .

When each jump operator is Hermitian, then from eqn. 1 we have that the infinite temperature state $\varrho \propto \mathbb{1}$ is a valid NESS. Furthermore, if H as well as all the jump operators commute with a set of independent projectors $\{P_s\}$ with $s \in \{1, \dots, K\}$, then any density matrix of the form

$$\varrho = c_0 \mathbb{1} + \sum_{s=1}^K c_s P_s \quad (2)$$

is also a valid NESS. This shall be the case for the model we investigate below. Thus we shall describe a system where there is relaxation to a degenerate block of NESSes. While such solutions to GKLS depend on the form of H and the jump operators $\{L_a\}$, they are independent of the various coupling constants (so long as they remain finite), and we shall consider them all to be infinite temperature states.

B. Equivalent non-Hermitian Hamiltonian

Any density matrix $\varrho = \sum_{m,n} \varrho_{mn} |m\rangle\langle n|$ may be represented in vector form as

$$\varrho \longrightarrow |\varrho\rangle \equiv \sum_{m,n} \varrho_{mn} |m\rangle \otimes |n\rangle. \quad (3)$$

Thus, the bra vector $\langle n|$ is replaced by the corresponding ket vector $|n\rangle$, *i.e.* $|m\rangle\langle n| \rightarrow |m\rangle \otimes |n\rangle$. If B is any operator, then under vectorization we have

$$\begin{aligned} \langle n|B &= \sum_k \langle n|B|k\rangle \langle k| \\ &\longrightarrow \sum_k |k\rangle \langle k|B^\top|n\rangle = B^\top|n\rangle. \end{aligned} \quad (4)$$

The GKLS master equation eqn. 1 then takes the vectorized form

$$i \frac{d}{dt} |\varrho\rangle = \mathcal{W} |\varrho\rangle, \quad (5)$$

where [12]

$$\begin{aligned} \mathcal{W} &= H \otimes \mathbb{1} - \mathbb{1} \otimes H^\top + \\ &+ i \sum_r \left(L_r \otimes L_r^* - \frac{1}{2} L_r^\dagger L_r \otimes \mathbb{1} - \mathbb{1} \otimes \frac{1}{2} L_r^\top L_r^* \right). \end{aligned} \quad (6)$$

Note that operators \mathcal{O} acting on the $|n\rangle$ component of the product $|m\rangle \otimes |n\rangle$ appear as transposes \mathcal{O}^\top , since they would normally act to the left on $\langle n|$. Eqn. 5 takes the form of an effective Schrödinger equation, with $|\varrho(t)\rangle$ evolving according to the non-Hermitian effective Hamiltonian \mathcal{W} acting on a doubled Hilbert space. For any operator \mathcal{O} , we may compute the trace in the vectorized representation according to

$$\text{Tr}(\mathcal{O}\varrho) = \langle \mathbb{I} | \mathcal{O} \otimes \mathbb{1} | \varrho \rangle, \quad (7)$$

where $\langle \mathbb{I} | = \sum_n \langle n | \otimes \langle n |$. The eigenvalues of \mathcal{W} , which we denote by $\{E_a\}$, are related to those of the Liouvillian by $E_a = i\Lambda_a$.

C. Shibata-Katsura Model

The Shibata-Katsura (SK) model [1] describes a dissipative $S = \frac{1}{2}$ chain. The Hamiltonian is

$$H = \sum_n (J_x X_{2n-1} X_{2n} + J_y Y_{2n} Y_{2n+1}) \quad (8)$$

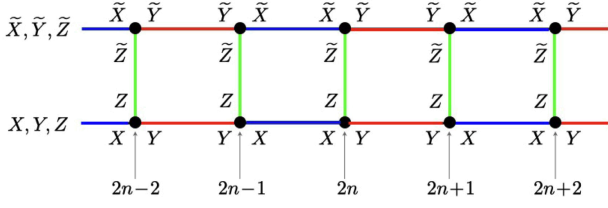


FIG. 1. The Shibata-Katsura ladder (see text for description).

and the jump operators are $L_n = \sqrt{\gamma} Z_n$, with $\gamma > 0$. Thus, we have

$$\mathcal{W}(\gamma) = \sum_{n=1}^{N_c} \left(J_x X_{2n-1} X_{2n} + J_y Y_{2n} Y_{2n+1} - J_x \tilde{X}_{2n-1} \tilde{X}_{2n} - J_y \tilde{Y}_{2n} \tilde{Y}_{2n+1} \right) + i\gamma \sum_{j=1}^N \left(Z_j \tilde{Z}_j - 1 \right) \quad , \quad (9)$$

where the (X, Y, Z) operators act on the first Hilbert space and $(\tilde{X}, \tilde{Y}, \tilde{Z})$ act on the copy. The system is depicted in Fig. 1 and corresponds to a non-Hermitian two-leg ladder. N_c is the number of unit cells, and there are $N = 2N_c$ sites on each leg of the ladder. Note that $\mathcal{W}^*(\gamma) = \mathcal{W}(-\gamma)$, and that if we define R as the reflection operator mapping one leg into the other, *i.e.* $(X_j, Y_j, Z_j) \leftrightarrow (\tilde{X}_j, \tilde{Y}_j, \tilde{Z}_j)$ for all j , then

$$R \mathcal{W}(\gamma) R = -\mathcal{W}(-\gamma) = -\mathcal{W}^*(\gamma) \quad . \quad (10)$$

This establishes that the eigenvalues of $\mathcal{W}(\gamma)$ come in pairs $\Lambda_a^\pm = \pm E_a + i\Gamma_a$. Total positivity requires that $\text{Im}(\Gamma_a) \leq 0$. Any NESS ϱ_{NESS} satisfies $\mathcal{W}(\gamma) | \varrho_{\text{NESS}} \rangle = 0$.

Introducing on each site four Majorana fermions $\theta^{0,1,2,3}$ and expressing the Pauli matrices therefrom,

$$X_j = i\theta_j^0 \theta_j^1 \quad , \quad Y_j = i\theta_j^0 \theta_j^2 \quad , \quad Z_j = i\theta_j^0 \theta_j^3 \quad , \quad (11)$$

with corresponding expression for $(\tilde{X}_j, \tilde{Y}_j, \tilde{Z}_j)$, one may express $\mathcal{W}(\gamma)$ as

$$\begin{aligned} \mathcal{W}(\gamma) = & \sum_{n=1}^{N_c} \left\{ iJ_x [\mu_{2n-1}^x \theta_{2n-1}^0 \theta_{2n}^0 - \tilde{\mu}_{2n-1}^x \tilde{\theta}_{2n-1}^0 \tilde{\theta}_{2n}^0] \right. \\ & \left. + iJ_y [\mu_{2n}^y \theta_{2n}^0 \theta_{2n+1}^0 - \tilde{\mu}_{2n}^y \tilde{\theta}_{2n}^0 \tilde{\theta}_{2n+1}^0] \right\} \\ & - \gamma \sum_{j=1}^N \mu_j^z \theta_j^0 \tilde{\theta}_j^0 - 2i\gamma N_c \quad , \end{aligned} \quad (12)$$

where

$$\begin{aligned} \mu_{2n-1}^x &= -i\theta_{2n-1}^1 \theta_{2n}^1 \quad , \quad \tilde{\mu}_{2n-1}^x = i\tilde{\theta}_{2n-1}^1 \tilde{\theta}_{2n}^1 \\ \mu_{2n}^y &= -i\theta_{2n}^2 \theta_{2n+1}^2 \quad , \quad \tilde{\mu}_{2n}^y = -i\tilde{\theta}_{2n}^2 \tilde{\theta}_{2n+1}^2 \quad , \quad \mu_j^z = -i\theta_j^3 \tilde{\theta}_j^3 \end{aligned} \quad (13)$$

are \mathbb{Z}_2 gauge fields on the links of the two leg ladder in fig. 1. These gauge fields commute with each other and with the θ^0 hopping terms, as well as with the constraints

$$\Lambda_j \equiv \theta_j^0 \theta_j^1 \theta_j^2 \theta_j^3 = +1 \quad , \quad \tilde{\Lambda}_j \equiv \tilde{\theta}_j^0 \tilde{\theta}_j^1 \tilde{\theta}_j^2 \tilde{\theta}_j^3 = +1 \quad . \quad (14)$$

which must be imposed at each site in order to guarantee $XY = iZ$. This is the magic of the Kitaev honeycomb lattice model, where the link lattice is also tripartite: the Hamiltonian corresponds to a single species (θ^0) of Majorana fermion hopping in the presence of a nondynamical \mathbb{Z}_2 gauge field. The gauge-invariant content of the theory is contained in the plaquette fluxes $\Phi_{2n-1} = \mu_{2n-1}^x \mu_{2n}^z \tilde{\mu}_{2n-1}^x \mu_{2n-1}^z$ and $\Phi_{2n} = \mu_{2n}^y \mu_{2n+1}^z \tilde{\mu}_{2n}^y \mu_{2n}^z$ and in the Wilson phases $Q = \prod_{j=1}^N Z_j$ and $\tilde{Q} = \prod_{j=1}^N \tilde{Z}_j$. With periodic boundary conditions, $Q\tilde{Q} = \prod_{j=1}^N \Phi_j$.

III. DIRAC MATRIX SK MODEL

A. Gamma matrix Kitaev models

A Clifford algebra is defined by the anticommutation relations,

$$\{\Gamma^a, \Gamma^b\} = 2\delta^{ab} \quad \mu, \nu \in \{1, \dots, n\} \quad . \quad (15)$$

When $n = 2k$, a representation of the algebra can be constructed by tensor products of k Pauli matrices, *viz.*

$$\begin{aligned} \Gamma^1 &= X \otimes \mathbb{1} \otimes \dots \otimes \mathbb{1} & \Gamma^{2k-1} &= Z \otimes Z \otimes \dots \otimes X \\ \Gamma^2 &= Y \otimes \mathbb{1} \otimes \dots \otimes \mathbb{1} & \Gamma^{2k} &= Z \otimes Z \otimes \dots \otimes Y \\ \Gamma^3 &= Z \otimes X \otimes \dots \otimes \mathbb{1} & \Gamma^{2k+1} &= Z \otimes Z \otimes \dots \otimes Z \end{aligned} \quad (16)$$

The gamma matrices defined above are all Hermitian. In even dimensions, we define

$$\Gamma^{2k+1} = (-i)^k \Gamma^1 \Gamma^2 \dots \Gamma^{2k} \quad . \quad (17)$$

Introducing $2k + 2$ Majorana fermions θ^a with indices $a \in \{0, \dots, 2k + 1\}$ satisfying $\{\theta^a, \theta^b\} = 2\delta^{ab}$, we define $\Gamma^\mu = i\theta^0 \theta^\mu$ with $\mu > 0$. Analogous to the constraint $\theta^0 \theta^1 \theta^2 \theta^3 = 1$ when $k = 1$, we demand

$$\theta^0 \theta^1 \dots \theta^{2k+1} = i^{k-1} \quad . \quad (18)$$

The case $k = 1$ yields the 2×2 Pauli matrices, with $\Gamma^1 = X$, $\Gamma^2 = Y$, and $\Gamma^3 = -i\Gamma^1 \Gamma^2 = Z$. The case $k = 2$ yields the 4×4 Dirac matrices, with $\Gamma^5 = -\Gamma^1 \Gamma^2 \Gamma^3 \Gamma^4$. For general k this yields $2k + 1$ matrices of rank 2^k . One can then form $\Gamma^{\mu\nu} = i\Gamma^\mu \Gamma^\nu = i\theta^\mu \theta^\nu$ of which there are $\binom{2k+1}{2}$ independent representatives (take $\mu < \nu$), and next $\Gamma^{\mu\nu\rho} = -i\Gamma^\mu \Gamma^\nu \Gamma^\rho = \theta^0 \theta^\mu \theta^\nu \theta^\rho$ and $\Gamma^\mu \Gamma^\nu \Gamma^\rho \Gamma^\sigma = \theta^\mu \theta^\nu \theta^\rho \theta^\sigma$, which yield $\binom{2k+1}{3}$ and $\binom{2k+1}{4}$ independent terms, respectively, *etc.* Proceeding thusly one obtains at level k a basis of 4^k Hermitian matrices of rank 2^k .

Analogs of Kitaev's honeycomb lattice model using these higher level Clifford algebras have been considered, *inter alia* in refs. [7, 8], with interactions $\Gamma_i^\mu \Gamma_j^\mu$ along the links. When the underlying lattice is such that each site lies at the confluence of $2k + 1$ distinctly labeled μ -links, the 'spin' Hamiltonian is again expressible as a single species (θ^0) Majorana fermion hopping in the presence of a static \mathbb{Z}_2 gauge field. Other generalizations, in which multiple species of Majoranas hop in the same \mathbb{Z}_2 static gauge field and hybridize as well have also been constructed [7, 13].

B. Dirac matrix SK model

We generalize the SK model to a dissipative Γ -matrix model defined on the square lattice, as depicted in fig. 2. We regard the square lattice as bipartite, with elementary direct lattice vectors $\mathbf{a}_{1,2} = \hat{\mathbf{x}} \pm \hat{\mathbf{y}}$. Our Hamiltonian is

$$H = \sum_{\mathbf{R}} \left(J_1 \Gamma_{\mathbf{R}}^1 \Gamma_{\mathbf{R}+\hat{\mathbf{x}}}^1 + J_2 \Gamma_{\mathbf{R}}^2 \Gamma_{\mathbf{R}+\hat{\mathbf{y}}}^2 + J_3 \Gamma_{\mathbf{R}}^3 \Gamma_{\mathbf{R}-\hat{\mathbf{x}}}^3 + J_4 \Gamma_{\mathbf{R}}^4 \Gamma_{\mathbf{R}-\hat{\mathbf{y}}}^4 \right), \quad (19)$$

where $\mathbf{R} = n_1 \mathbf{a}_1 + n_2 \mathbf{a}_2$ with $n_{1,2} \in \mathbb{Z}$ are the A sublattice sites, which are N_c in number. We use the symbol \mathbf{r} to denote a site which may be in either sublattice. Thus, on each site of the square lattice, a four-dimensional Hilbert space is acted upon by operators $1_{\mathbf{r}}$, $\Gamma_{\mathbf{r}}^\mu$, and $\Gamma_{\mathbf{r}}^{\mu\nu}$, where Γ^μ are 4×4 Dirac matrices, with $\mu \in \{1, \dots, 5\}$.

Following SK, we take the Lindblad jump operators to be $L_{\mathbf{r}} = \sqrt{\gamma} \Gamma_{\mathbf{r}}^5$ at each site. The GKLS master equation can then be written as a non-Hermitian Hamiltonian evolution of a model on a square lattice bilayer, with each layer corresponding to one copy of the Hilbert space. This Hamiltonian is

$$\mathcal{W}(\{J_\delta\}, \gamma) = \sum_{\mathbf{R} \in \text{A}} \sum_{\delta=1}^4 J_\delta \left(i u_{\mathbf{R}}^\delta \theta_{\mathbf{R}}^0 \theta_{\mathbf{R}+\delta}^0 - i \tilde{u}_{\mathbf{R}}^\delta \tilde{\theta}_{\mathbf{R}}^0 \tilde{\theta}_{\mathbf{R}+\delta}^0 \right) - \gamma \sum_{\mathbf{r} \in \text{A,B}} u_{\mathbf{r}}^5 \theta_{\mathbf{r}}^0 \tilde{\theta}_{\mathbf{r}}^0 - 2i\gamma N_c, \quad (20)$$

where $\delta \in \{\hat{\mathbf{x}}, \hat{\mathbf{y}}, -\hat{\mathbf{x}}, -\hat{\mathbf{y}}\}$ for $\delta \in \{1, 2, 3, 4\}$, respectively, and where (see fig. 3)

$$u_{\mathbf{R}}^\delta = -i\theta_{\mathbf{R}}^\delta \theta_{\mathbf{R}+\delta}^\delta, \quad \tilde{u}_{\mathbf{R}}^\delta = -i\tilde{\theta}_{\mathbf{R}}^\delta \tilde{\theta}_{\mathbf{R}+\delta}^\delta, \quad u_{\mathbf{r}}^5 = -i\theta_{\mathbf{r}}^5 \tilde{\theta}_{\mathbf{r}}^5 \quad (21)$$

are the nondynamical gauge fields in the bottom, top, and between layer regions. There are $5N$ such gauge fields, but as we shall see the number of gauge-invariant quantities is $3N + 1$, *i.e.* there are 2^{3N+1} gauge sectors, where N is the total number of sites in either layer.

1. Conserved quantities

For the original SK model, the product $Q = Z_1 \cdots Z_N$ is conserved as it commutes with H and with each of the jump operators $\sqrt{\gamma} Z_j$. This means that both 1 and Q are annihilated by the Liouvillian \mathcal{L} , and that both

$$\varrho_{\pm} = 2^{-N} (1 \pm Q) \quad (22)$$

are thus valid NESSes, for all γ [1].

For our model of eqn. 20, there are vastly more conserved quantities. With periodic boundary conditions along both axes, there are $N + 1$ gauge-invariant quantities, which are the N plaquette fluxes (see fig. 2),

$$\Phi_{\mathbf{r}} \equiv \begin{cases} -\Gamma_{\mathbf{r}}^{21} \Gamma_{\mathbf{r}+\hat{\mathbf{x}}}^{14} \Gamma_{\mathbf{r}+\hat{\mathbf{x}}+\hat{\mathbf{y}}}^{43} \Gamma_{\mathbf{r}+\hat{\mathbf{y}}}^{32} & \text{if } \mathbf{r} \in \text{A} \\ -\Gamma_{\mathbf{r}}^{43} \Gamma_{\mathbf{r}+\hat{\mathbf{x}}}^{32} \Gamma_{\mathbf{r}+\hat{\mathbf{x}}+\hat{\mathbf{y}}}^{21} \Gamma_{\mathbf{r}+\hat{\mathbf{y}}}^{14} & \text{if } \mathbf{r} \in \text{B} \end{cases}, \quad (23)$$

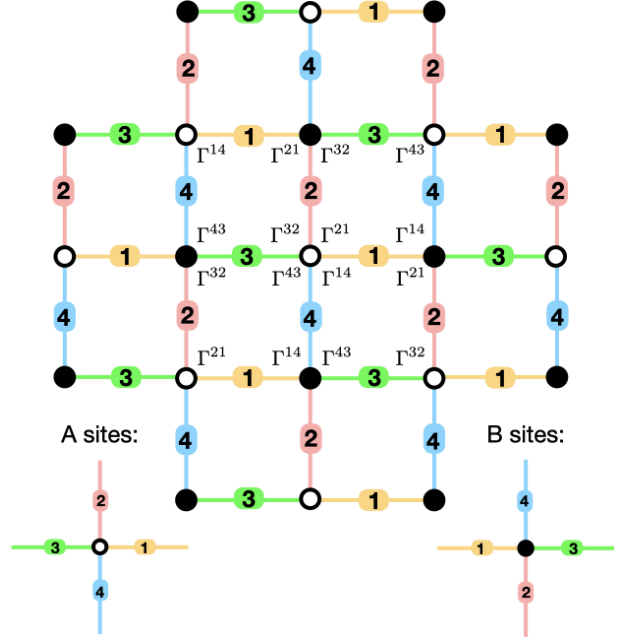


FIG. 2. Square lattice Dirac matrix Shibata-Katsura model. See description in §III C.

where the \mathbb{Z}_2 flux in plaquette \mathbf{r} is labeled by the lower left site of the plaquette [14]. Note that the product $\prod_{\mathbf{r}} \Phi_{\mathbf{r}} = 1$, hence there are $N - 1$ independent \mathbb{Z}_2 plaquette fluxes. In addition, we have the two Wilson phases,

$$W_x = -\Gamma_{1,1}^{13} \Gamma_{2,1}^{31} \cdots \Gamma_{N_x-1,1}^{13} \Gamma_{N_x,1}^{31} \quad (24)$$

$$W_y = -\Gamma_{1,1}^{24} \Gamma_{1,2}^{42} \cdots \Gamma_{1,N_y-1}^{24} \Gamma_{1,N_y}^{42},$$

where both N_x and N_y are taken to be even, and with the total number of sites $N \equiv N_x N_y$. (Note that $\Gamma^{31} = -\Gamma^{13}$ and $\Gamma^{42} = -\Gamma^{23}$; we choose to write the Wilson phases as above because the repetition of consecutive Γ -matrix indices is a useful mnemonic.) One can readily check that $\Phi_{\mathbf{r}}$ commutes with both H and with all the jump operators. In addition, the operator $Q = \prod_{\mathbf{r}} \Gamma_{\mathbf{r}}^5$ also commutes with the Hamiltonian and with all of the jump operators. However, if we examine the product of the \mathbb{Z}_2 fluxes over the A plaquettes alone, *i.e.* over those plaquettes with an A site in their lower left corner, then from $\Gamma^{43} \Gamma^{21} = -\Gamma^{13} \Gamma^{23} \Gamma^{34} = \Gamma^5$, we conclude that $\prod_{\mathbf{R} \in \text{A}} \Phi_{\mathbf{R}} = \prod_{\mathbf{r}} \Gamma_{\mathbf{r}}^5 = Q$, and therefore Q is not an independent conserved quantity. Finally, as the jump operators are all Hermitian, according to eqn. 2 we have a 2^{N+1} -dimensional subspace of $T = \infty$ nonequilibrium steady states, since there are 2^{N+1} projectors,

$$\Pi_{\eta_x, \eta_y, \{\eta_{\mathbf{r}}\}} \equiv \left(\frac{1 + \eta_x W_x}{2} \right) \left(\frac{1 + \eta_y W_y}{2} \right) \times \prod_{\mathbf{r}} \left(\frac{1 + \eta_{\mathbf{r}} \Phi_{\mathbf{r}}}{2} \right), \quad (25)$$

labeled by η_x , η_y , and $\{\eta_{\mathbf{r}}\}$, each taking the value ± 1 , which commute with H and with all the jump operators

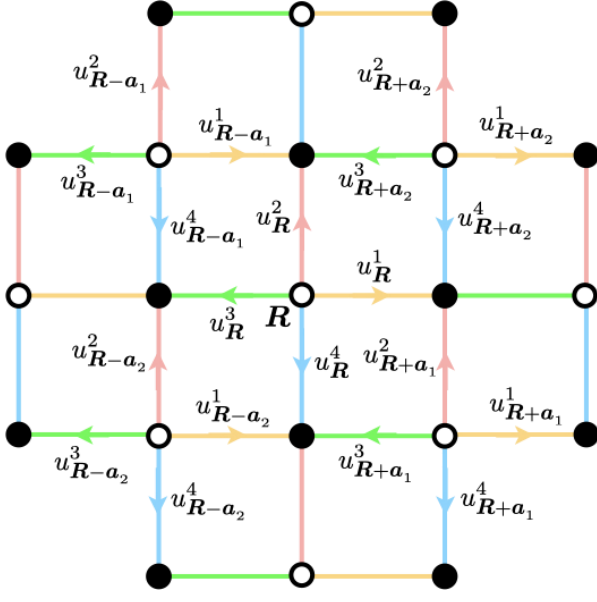


FIG. 3. At each A sublattice site in the bottom layer, the gauge field u_R^δ points along the nearest neighbor vector δ toward a neighboring B sublattice site. A corresponding convention pertains for the \tilde{u}_R^δ gauge fields in the top layer.

L_r . The prime on the product indicates that the final plaquette with $\mathbf{r} = (N_x, N_y)$ is omitted. The total number of unnormalized density matrices is $(4^2)^N = 16^N$. *I.e.* any density matrix of the form

$$\varrho = \sum_{\eta_x} \sum_{\eta_y} \sum_{\{\eta_r\}} C_{\eta_x, \eta_y, \{\eta_r\}} \Pi_{\eta_x, \eta_y, \{\eta_r\}} \quad (26)$$

with $\text{Tr } \varrho = \sum_{\eta_x} \sum_{\eta_y} \sum_{\{\eta_r\}} C_{\eta_x, \eta_y, \{\eta_r\}} = 1$ and each $C_{\eta_x, \eta_y, \{\eta_r\}} \geq 0$ is a valid NESS.

C. Analysis

We define a complex fermion living along each link between planes of the bilayer, *viz.*

$$c_r = \frac{1}{2}(\theta_r^0 + i\tilde{\theta}_r^0) \quad , \quad c_r^\dagger = \frac{1}{2}(\theta_r^0 - i\tilde{\theta}_r^0) \quad , \quad (27)$$

and thus

$$\theta_r^0 = c_r^\dagger + c_r \quad , \quad \tilde{\theta}_r^0 = i(c_r^\dagger - c_r) \quad . \quad (28)$$

The non-Hermitian Hamiltonian of eqn. 20 is then expressed in terms of these complex fermions as

$$\begin{aligned} \mathcal{W} = \sum_{R \in A} \sum_{\delta=1}^4 \left\{ iJ_\delta (u_R^\delta - \tilde{u}_R^\delta) (c_{R+C_R+\delta}^\dagger + c_{R+\delta}^\dagger c_R) \right. \\ \left. + iJ_\delta (u_R^\delta + \tilde{u}_R^\delta) (c_{R+C_R+\delta}^\dagger - c_{R+\delta}^\dagger c_R) \right\} \\ + i\gamma \sum_{r \in A, B} u_r^5 (2c_r^\dagger c_r - 1) - 2iN_c \gamma \quad . \end{aligned} \quad (29)$$

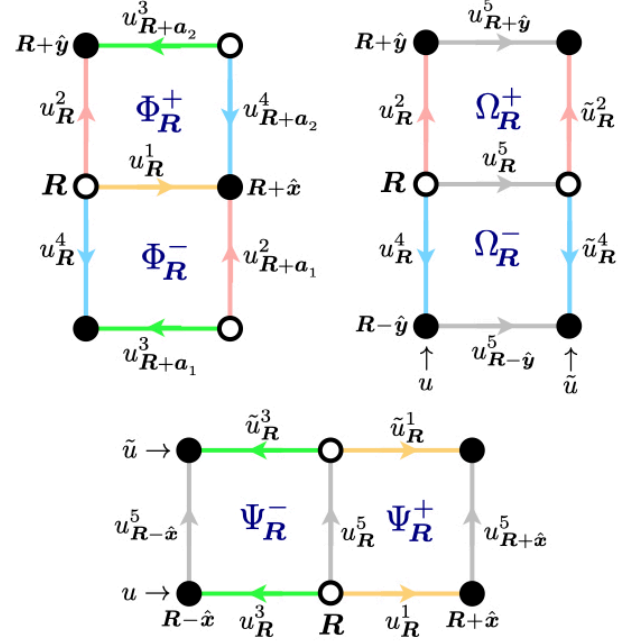


FIG. 4. Associated with each A sublattice site in the bottom layer are eight square plaquette fluxes: Φ_R^\pm , $\tilde{\Phi}_R^\pm$ (not shown), Ψ_R^\pm , and Ω_R^\pm .

D. Counting degrees of freedom

Associated with each A sublattice site in the bottom layer are eight square plaquette \mathbb{Z}_2 fluxes (see fig. 4). These fall into three groups. First are the fluxes through the (x, y) plaquettes. For the bottom layer we have

$$\begin{aligned} \Phi_R^+ &= u_R^1 u_{R+a_2}^4 u_{R+a_2}^3 u_R^2 = -\Gamma_R^{21} \Gamma_{R+\hat{x}}^{14} \Gamma_{R+a_2}^{43} \Gamma_{R+\hat{y}}^{32} \\ \Phi_R^- &= u_R^4 u_{R+a_1}^3 u_{R+a_1}^2 u_R^1 = -\Gamma_R^{14} \Gamma_{R-\hat{y}}^{43} \Gamma_{R+a_1}^{32} \Gamma_{R+\hat{x}}^{21} \end{aligned} \quad (30)$$

with corresponding expressions involving $\tilde{\Phi}_R^\pm$, $\tilde{\Gamma}_r$, and \tilde{u}_R^δ in the top layer. Next, the (x, z) plaquette fluxes Ψ_R^\pm ,

$$\begin{aligned} \Psi_R^+ &= u_R^1 u_{R+\hat{x}}^5 \tilde{u}_R^1 u_R^5 = -\Gamma_R^{51} \Gamma_{R+\hat{x}}^{15} \tilde{\Gamma}_{R+\hat{x}}^{51} \tilde{\Gamma}_R^{15} \\ \Psi_R^- &= u_R^5 \tilde{u}_R^3 u_{R-\hat{x}}^5 u_R^3 = -\Gamma_R^{35} \Gamma_R^{53} \tilde{\Gamma}_{R-\hat{x}}^{35} \tilde{\Gamma}_{R-\hat{x}}^{53} \quad . \end{aligned} \quad (31)$$

Finally, the (y, z) plaquette fluxes Ω_R^\pm are given by

$$\begin{aligned} \Omega_R^+ &= u_R^2 u_{R+\hat{y}}^5 \tilde{u}_R^2 u_R^5 = -\Gamma_R^{52} \Gamma_{R+\hat{y}}^{25} \tilde{\Gamma}_{R+\hat{y}}^{52} \tilde{\Gamma}_R^{25} \\ \Omega_R^- &= u_R^5 \tilde{u}_R^4 u_{R-\hat{y}}^5 u_R^4 = -\Gamma_R^{45} \tilde{\Gamma}_R^{54} \tilde{\Gamma}_{R-\hat{y}}^{45} \Gamma_{R-\hat{y}}^{54} \quad . \end{aligned} \quad (32)$$

There are also the Wilson phases,

$$\begin{aligned} W_x &= u_{1,1}^1 (-u_{3,1}^3) u_{3,1}^1 (-u_{5,1}^3) \cdots u_{N_x-1,1}^1 (-u_{1,1}^3) \\ &= -\Gamma_{1,1}^{13} \Gamma_{2,1}^{31} \cdots \Gamma_{N_x,1}^{31} \\ W_y &= u_{1,1}^2 (-u_{1,3}^4) u_{1,3}^2 (-u_{1,5}^4) \cdots u_{1,N_y-1}^2 (-u_{1,1}^4) \\ &= \Gamma_{1,1}^{24} \Gamma_{1,2}^{42} \cdots \Gamma_{1,N_y}^{42} \quad , \end{aligned} \quad (33)$$

again with corresponding expressions for \widetilde{W}_x and \widetilde{W}_y . At this point it appears that we have $4N + 4$ gauge-invariant \mathbb{Z}_2 degrees of freedom. However, the total flux through each of the N cubes must be trivial, providing N constraints. There is an additional constraint $\prod_{\mathbf{R}} \Phi_{\mathbf{R}}^+ \Phi_{\mathbf{R}}^- = 1$ due to periodic boundary conditions; the corresponding expression in the top layer does not yield new information given the condition on each of the cubes. Finally, there are two constraints relating the products of the Wilson phases in each of the layers to the Ω and Ψ plaquette fluxes (see eqn. 41 below.) Thus, there are $N + 3$ independent constraints, and therefore $3N + 1$ independent gauge-invariant configurations of the fluxes and Wilson phases. We must also acknowledge the constraints imposed by the projectors which enforce $\Lambda_{\mathbf{r}} = \widetilde{\Lambda}_{\mathbf{r}} = 1$, with $\Lambda_{\mathbf{r}} = \theta_{\mathbf{r}}^0 \theta_{\mathbf{r}}^1 \theta_{\mathbf{r}}^2 \theta_{\mathbf{r}}^3 \theta_{\mathbf{r}}^4 \theta_{\mathbf{r}}^5 = -i$. Taking the product over all sites, we obtain [7]

$$\prod_{\mathbf{r}} i \theta_{\mathbf{r}}^0 \widetilde{\theta}_{\mathbf{r}}^0 \times \prod_{\mathbf{R}, \delta} u_{\mathbf{R}}^{\delta} \widetilde{u}_{\mathbf{R}}^{\delta} \times \prod_{\mathbf{r}} u_{\mathbf{r}}^5 = 1 \quad . \quad (34)$$

This expression includes a product over all the itinerant fermion parities $2c_{\mathbf{r}}^{\dagger} c_{\mathbf{r}} - 1$ as well as over each of the $5N$ \mathbb{Z}_2 gauge fields which reside on the links of the bilayer structure. It thereby constrains the parity of the c -fermions, which are constructed from θ^0 and $\widetilde{\theta}^0$ on each of the interplane links. Thus rather than N freedoms for the dynamical fermion states, there are $N - 1$, and the total number of states in our doubled Hilbert space is $2^{3N+1} \times 2^{N-1} = 16^N$, which is the correct number of density matrices for an N -site system described by 4×4 gamma matrices [15].

E. Choosing a gauge

Given the $3N + 1$ independent plaquette fluxes and Wilson phases, how can we pick a gauge? Let us first consider the planar fluxes $\Phi_{\mathbf{R}}^{\pm}$ in the bottom layer and the sketch in fig. 5. The coordinates of the A sublattice site in the lower left corner are $\mathbf{r} = (x, y) = (1, 1)$. The Wilson phase fluxes are defined to be $u_{1,1}^1 \equiv W_x$ and $u_{1,1}^4 \equiv -W_y$. We then define the remaining unassigned gauge fields as follows:

$$\begin{aligned} u_{2,2}^3 &= \Phi_{1,1}^+ u_{1,1}^1 & u_{2,2}^1 &= \Phi_{2,2}^- \\ u_{1,3}^1 &= \Phi_{1,3}^- u_{2,2}^3 & u_{3,3}^3 &= \Phi_{2,2}^+ u_{2,2}^1 \quad \dots \\ u_{1,N_y-1}^1 &= \Phi_{1,N_y-1}^- u_{2,N_y-2}^3 & u_{3,N_y-1}^3 &= \Phi_{2,N_y-2}^+ u_{2,N_y-2}^1 \\ u_{2,N_y}^3 &= \Phi_{1,N_y-1}^+ u_{1,N_y-1}^1 & u_{2,N_y}^1 &= \Phi_{2,N_y}^- u_{3,N_y-1}^3 \\ u_{2,N_y}^2 &= \Phi_{1,1}^- u_{1,1}^4 u_{2,N_y}^3 & u_{3,1}^4 &= \Phi_{2,N_y}^- u_{2,N_y}^1 u_{2,N_y}^2 \end{aligned}$$

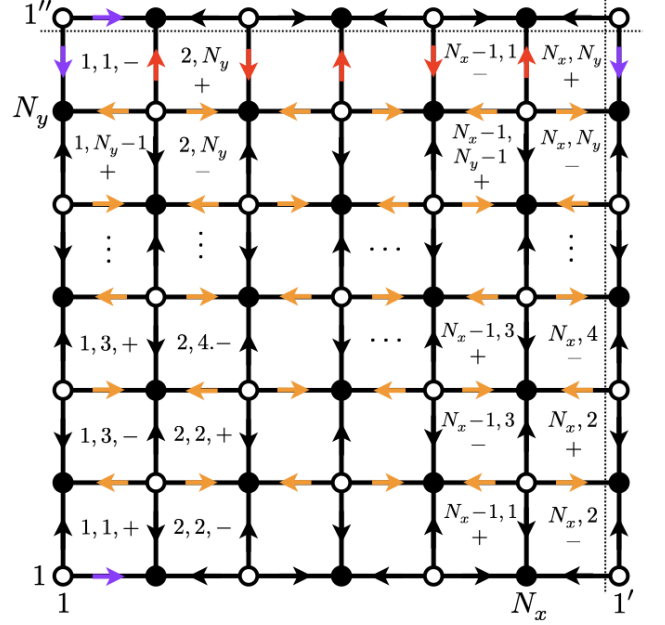


FIG. 5. Labels of the unit cells $\Phi_{\mathbf{R}}^{\pm}$. The black arrows indicate $u_{\mathbf{R}}^{\delta} = +1$ in the direction of the arrow. There are $N + 1$ colored arrows, which are determined by the $N - 1$ independent plaquette fluxes and the two Wilson loops. A corresponding assignment pertains to the upper layer with fluxes $\Phi_{\mathbf{R}}^{\pm}$ and gauge fields $\widetilde{u}_{\mathbf{R}}^{\delta}$. Dotted lines indicate periodicity boundaries.

and

$$\begin{aligned} u_{4,2}^3 &= \Phi_{3,1}^+ & u_{N_x,2}^1 &= \Phi_{N_x,2}^- & (35) \\ u_{3,3}^1 &= \Phi_{3,3}^- u_{4,2}^3 & u_{1,3}^3 &= \Phi_{N_x,2}^+ u_{N_x,2}^1 \\ u_{4,4}^3 &= \Phi_{3,3}^+ u_{3,3}^1 & u_{N_x,4}^1 &= \Phi_{N_x,4}^- u_{1,3}^3 \quad \dots \\ u_{3,N_y-1}^1 &= \Phi_{3,N_y-1}^- u_{4,N_y-2}^3 & u_{1,N_y-1}^3 &= \Phi_{N_x,N_y-2}^+ u_{N_x,N_y-2}^1 \\ u_{4,N_y}^3 &= \Phi_{3,N_y-1}^+ u_{3,N_y-1}^1 & u_{N_x,N_y}^1 &= \Phi_{N_x,N_y}^- u_{1,N_y-1}^3 \\ u_{3,1}^4 &= \Phi_{2,N_y}^+ u_{2,N_y}^3 u_{2,N_y}^1 & u_{1,1}^4 &= -W_y \quad . \end{aligned}$$

Thus, we can iteratively obtain all the unassigned \mathbb{Z}_2 gauge fields $u_{\mathbf{R}}^{\delta}$ from the plaquette phases and the Wilson phases. Again, corresponding expressions hold in the upper layer for the quantities $\{\widetilde{u}_{\mathbf{R}}^{\delta}, \Phi_{\mathbf{R}}^{\pm}, \widetilde{W}_x, \widetilde{W}_y\}$.

Next, we consider the $u_{\mathbf{R}}^5$ gauge fields and the plaquette fluxes $\{\Psi_{\mathbf{R}}^{\pm}, \Omega_{\mathbf{R}}^{\pm}\}$. From eqn. 30 we may iteratively determine the values of $u_{m,k}^5$ for odd values of k given the value $u_{1,k}^5 \equiv 1$:

$$\begin{aligned} u_{2,k}^5 &= u_{1,k}^1 \widetilde{u}_{1,k}^1 \Psi_{1,k}^+ \cdot u_{1,k}^5 & (36) \\ u_{3,k}^5 &= u_{3,k}^3 \widetilde{u}_{3,k}^3 \Psi_{3,k}^- \cdot u_{2,k}^5 \\ u_{4,k}^5 &= u_{3,k}^1 \widetilde{u}_{3,k}^1 \Psi_{3,k}^+ \cdot u_{3,k}^5 \quad \dots \\ u_{N_x,k}^5 &= u_{N_x-1,k}^1 \widetilde{u}_{N_x-1,k}^1 \Psi_{N_x-1,k}^+ \cdot u_{N_x-1,k}^5 \\ u_{1,k}^5 &= u_{1,k}^1 \widetilde{u}_{1,k}^1 \Psi_{1,k}^- \cdot u_{N_x,k}^5 \quad . \end{aligned}$$

For even values of k , we have

$$\begin{aligned}
u_{2,k}^5 &= u_{2,k}^3 \tilde{u}_{2,k}^3 \Psi_{2,k}^- \cdot u_{1,k}^5 \\
u_{3,k}^5 &= u_{2,k}^1 \tilde{u}_{2,k}^1 \Psi_{2,k}^+ \cdot u_{2,k}^5 \\
u_{4,k}^5 &= u_{4,k}^3 \tilde{u}_{4,k}^3 \Psi_{4,k}^- \cdot u_{3,k}^5 \quad \dots \\
u_{N_x,k}^5 &= u_{N_x,k}^3 \tilde{u}_{N_x,k}^3 \Psi_{N_x,k}^- \cdot u_{N_x-1,k}^5 \\
u_{1,k}^5 &= u_{N_x,k}^1 \tilde{u}_{N_x,k}^1 \Psi_{N_x,k}^+ \cdot u_{N_x,k}^5 \quad .
\end{aligned} \tag{37}$$

To obtain $u_{1,k+1}^5$ from $u_{1,k}^5$, we use the relations

$$\begin{aligned}
u_{1,2n}^5 &= u_{1,2n-1}^2 \tilde{u}_{1,2n-1}^2 \Omega_{1,2n-1}^+ \cdot u_{1,2n-1}^5 \\
u_{1,2n+1}^5 &= u_{1,2n}^4 \tilde{u}_{1,2n}^4 \Omega_{1,2n+1}^- \cdot u_{1,2n}^5 \quad .
\end{aligned} \tag{38}$$

Eqns. 36, 37, and 38 entail the relations

$$\begin{aligned}
\prod_{\substack{j=1 \\ (k \text{ odd})}}^{N_x} \Psi_{j,k}^- \Psi_{j,k}^+ &= \prod_{m=1}^{N_x/2} u_{2m-1,k}^1 u_{2m-1,k}^3 \tilde{u}_{2m-1,k}^1 \tilde{u}_{2m-1,k}^3 \\
\prod_{\substack{j=1 \\ (k \text{ even})}}^{N_x} \Psi_{j,k}^- \Psi_{j,k}^+ &= \prod_{m=1}^{N_x/2} u_{2m,k}^1 u_{2m,k}^3 \tilde{u}_{2m,k}^1 \tilde{u}_{2m,k}^3 \quad , \tag{39}
\end{aligned}$$

for k odd and even, respectively, as well as

$$\begin{aligned}
\prod_{\substack{k=1 \\ (j \text{ odd})}}^{N_y} \Omega_{j,k}^- \Omega_{j,k}^+ &= \prod_{n=1}^{N_y/2} u_{j,2n-1}^2 u_{j,2n-1}^4 \tilde{u}_{j,2n-1}^2 \tilde{u}_{j,2n-1}^4 \\
\prod_{\substack{k=1 \\ (j \text{ even})}}^{N_y} \Omega_{j,k}^- \Omega_{j,k}^+ &= \prod_{n=1}^{N_y/2} u_{j,2n}^2 u_{j,2n}^4 \tilde{u}_{j,2n}^2 \tilde{u}_{j,2n}^4 \quad , \tag{40}
\end{aligned}$$

for j odd and even, respectively. Restricting to the cases $j = 1$ and $k = 1$, we can relate these products to the Wilson phases in eqn. 33, *viz.*

$$\begin{aligned}
\prod_{k=1}^{N_y} \Omega_{1,k}^- \Omega_{1,k}^+ &= W_x \widetilde{W}_x \\
\prod_{j=1}^{N_x} \Psi_{j,1}^- \Psi_{j,1}^+ &= W_y \widetilde{W}_y \quad .
\end{aligned} \tag{41}$$

We showed previously in §III D that, considering all the \mathbb{Z}_2 gauge degrees of freedom, we have a total of $3N + 1$ independent plaquette fluxes and Wilson phases. In each layer, there are $N + 1$ free gauge fields $u_{\mathbf{R}}^\delta$, as depicted in fig. 5. Between the layers, there are $N - 1$ free gauge fields $u_{\mathbf{r}}^5$, with $u_{1,1}^5 \equiv 1$. Thus, our gauge assignment accounts for all the independent gauge-invariant quantities.

F. Counting the NESSes

Referring to eqn. 29, in order to obtain an eigenvalue of zero, we must have each $u_{\mathbf{r}}^5 = +1$ and $c_{\mathbf{r}}^\dagger c_{\mathbf{r}} = 1$. (The

case $u_{\mathbf{r}}^5 = -1$ for all \mathbf{r} is impossible since we have, without loss of generality (*i.e.* up to a gauge transformation), set $u_{1,1}^5 \equiv 1$.) We then must eliminate the BCS pairing terms, which would allow for the simultaneous annihilation of two neighboring c -fermions. This is accomplished by setting $u_{\mathbf{R}}^\delta + \tilde{u}_{\mathbf{R}}^\delta = 0$ for all \mathbf{R} and δ . While this may seem inconsistent with the assignment of the fixed gauge fields (black arrows) in the two layers as depicted in fig. 5, in fact we are free to redefine $\tilde{u}_{\mathbf{R}}^\delta \rightarrow -\tilde{u}_{\mathbf{R}}^\delta$ for the purposes of counting the NESSes. Thus, there are a total of $N + 1$ independent values of the planar ($\delta \in \{1, 2, 3, 4\}$) gauge fields associated with the NESS block, and therefore 2^{N+1} degenerate NESSes.

It can be seen that for these NESSes $\Phi_{\mathbf{R}}^+ = \tilde{\Phi}_{\mathbf{R}}^+$ and $\Phi_{\mathbf{R}}^- = \tilde{\Phi}_{\mathbf{R}}^-$, as well as $\Psi_{\mathbf{R}}^+ = \Psi_{\mathbf{R}}^- = -1$ and $\Omega_{\mathbf{R}}^+ = \Omega_{\mathbf{R}}^- = -1$, for all \mathbf{R} . Since $\prod_{\mathbf{R}} \Phi_{\mathbf{R}}^+ \Phi_{\mathbf{R}}^- = 1$, this accounts for $N - 1$ freedoms associated with the plaquette fluxes. The Wilson phases W_x and W_y are also free (but \widetilde{W}_x and \widetilde{W}_y are then fixed by eqn. 41), and so again we see that there are 2^{N+1} NESSes.

We numerically verified this counting for the case $N_x = N_y = 2$ ($N = 4$) by choosing the J_δ couplings to be all different. However, when $J_1 = J_2 = J_3 = J_4$ there is an enlarged translational symmetry, and we find a degeneracy of 90 rather than $2^{N+1} = 32$. We also find that these additional degenerate states do not satisfy the flux conditions described in the previous paragraph.

IV. COMPUTATIONAL RESULTS

To calculate the spectrum within a given gauge sector, we use Prosen's method for complex antisymmetric matrices [4]. We note that the constraint in equation 34 is implemented as a constraint on the parity of the complex fermions that arise from Prosen's generalized Bogoliubov transformation.

Implementing the field assignments mentioned in section III E, we calculate the gap g to the smallest relaxation rate, *i.e.* the negative of the real part of the eigenvalues of \mathcal{L} , by searching over all the sectors of the \mathcal{L} corresponding to the different plaquette flux and Wilson phase configurations, for the case $N_x = N_y = 2$. For this system there are $N = 4$ sites and thus 2^{16} (unnormalized) density matrices. We observe a transition in the first decay modes. The plot showing g as a function of γ for $J_1 = J_2 = J_3 = J_4 = 1$ is shown in fig. 6. The gauge-invariant quantities corresponding to the first decay modes are shown in figures 7 and 8.

The results obtained from $N_x = N_y = 2$ system could be subject to finite-size effects. Hence we proceed to estimate the gap for higher system sizes, using other methods to optimize for the gap since it is computationally intensive to examine all 2^{3N+1} of the gauge sectors. We first tried looking at all configurations with a fixed number N_v of \mathbb{Z}_2 defects – plaquettes and Wilson phases whose values are reversed relative to a given NESS configuration.

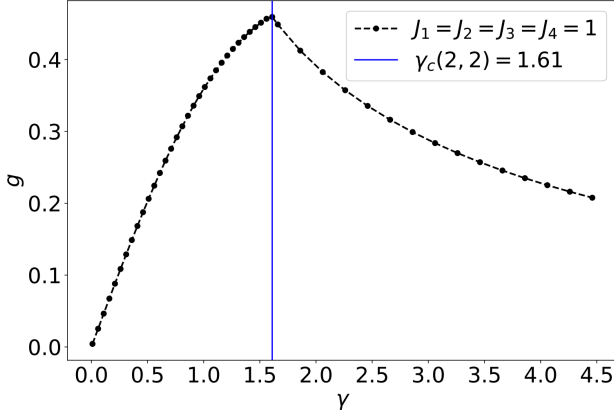


FIG. 6. Liouvillian gap in the 2d generalized SK model with periodic boundary conditions for $N_x = N_y = 2$ and all $J_\delta = 1$: The Liouvillian gap, g , as a function of γ . There is a transition in the first decay modes at the cusp seen at $\gamma = \gamma_c(2, 2)$, depicted by the blue vertical line.

(A reversed-flux plaquette is a \mathbb{Z}_2 vortex.) There being $N_g = 3N + 1$ gauge degrees of freedom, the number of such configurations ($\binom{N_g}{N_v}$) rapidly becomes computationally unwieldy with growing N_g and N_v . We searched exhaustively for the smallest nonzero relaxation rates for up to $N_v = 4$ total \mathbb{Z}_2 defects for $N_x = N_y = 4$ and only up to $N_v = 2$ for $N_x = N_y = 6$ relative to a particular NESS (one with all gauge-invariant \mathbb{Z}_2 data set to

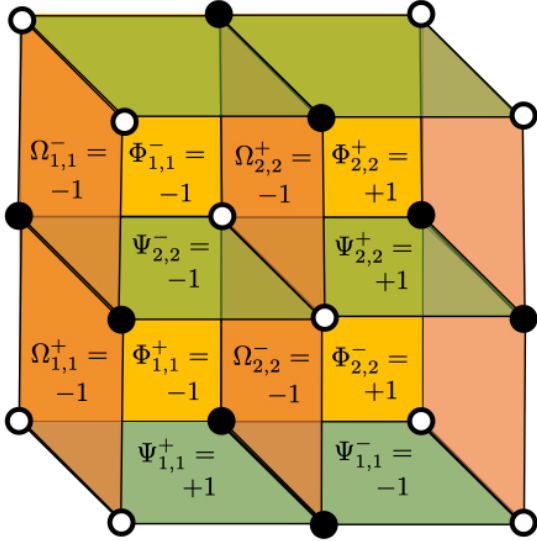


FIG. 7. A first decay mode of the 2d generalized SK model with periodic boundary conditions for $N_x = N_y = 2$ and $J_1 = J_2 = J_3 = J_4 = 1$ corresponding to the ‘phase’ where $\gamma \leq \gamma_c(2, 2)$. For the mode shown in this figure, we have $W_x = 1, W_y = -1, \tilde{W}_x = -1, \tilde{W}_y = -1$. There are 15 other configurations of the flux plaquettes and Wilson phases corresponding to the same eigenvalue as the first decay mode shown here.

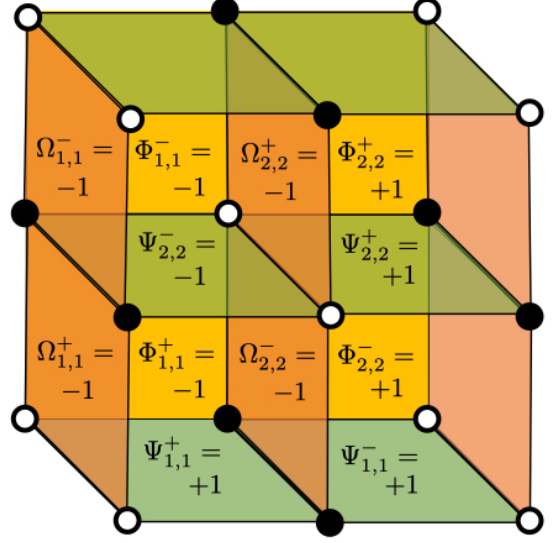


FIG. 8. A first decay mode of the 2d generalized SK model with periodic boundary conditions for $N_x = N_y = 2$ and $J_1 = J_2 = J_3 = J_4 = 1$ corresponding to the ‘phase’ where $\gamma \geq \gamma_c(2, 2)$. For the mode shown in this figure, we have $W_x = 1, W_y = -1, \tilde{W}_x = 1, \tilde{W}_y = -1$. There are 79 other configurations of the flux plaquettes and Wilson phases corresponding to the same eigenvalue as the first decay mode shown here.

–1). We also performed a Monte Carlo searches using both simulated annealing and a genetic algorithm (GA) capable of finding states with arbitrary numbers of defects. These both yielded similar results, and below we show data only for the GA computations when comparing with the N_v -limited searches.

Some details regarding the GA are provided in §B below. We found the results to be satisfactory both in terms of convergence of the longest nonzero relaxation rate g as well as the computational run time for systems up to size 6×6 (2^{144} density matrices). We cannot estimate the full spectrum of first decay modes through this method, *i.e.* enumerating all their degeneracies as in the 2×2 case, however. The results obtained by taking the minimum value from different runs (see §B) of the genetic algorithm are shown in fig. 9. The result for $N_x = N_y = 6$ is subject to more error since we used a fewer number of runs than in the 4×4 case. This estimate can be improved by using the decay modes obtained from the genetic algorithm.

To obtain better estimates, we collect the best individuals from different GA runs (field configurations with minimum gap, *i.e.* the configurations corresponding to g_{\min} in fig. 22 in B), and for different values of γ . We then use this set of field configurations as our pool to be tried for each value of γ in order to obtain an estimate of the minimum gap, g , by optimizing the relaxation rate gap with respect to allowed configurations. This yields the curve labeled GA in fig. 10. For the system sizes we have examined, the $g(\gamma)$ curves all exhibit a linear behav-

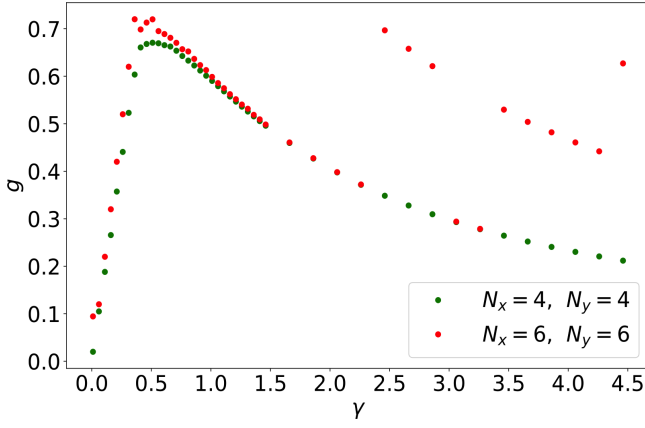


FIG. 9. Minimal relaxation rate g versus γ obtained over different runs of the genetic algorithm (all $J_\delta = 1$) for 4×4 and 6×6 system sizes. The population size was 100 and the number of runs was 10 for 4×4 and 5 for 6×6 .

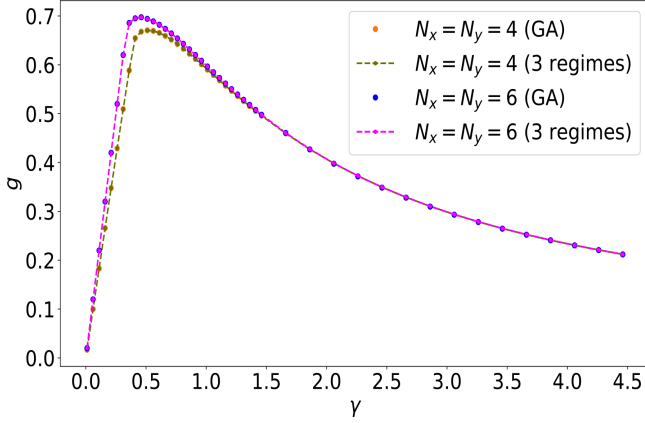


FIG. 10. GA and the regimes are described in the text. All $J_\delta = 1$. The regimes for size 4×4 are given by $\gamma < 0.41$, $\gamma = 0.41$ (a single point) and $\gamma > 0.41$. The regimes for size 6×6 are separated at $\gamma_1^* = 0.36$ and $\gamma_2^* = 0.41$.

ior at small γ , crossing over to a $1/\gamma$ behavior at large γ , as found by SK for their model [1]. While the gauge configurations obtained in this manner can vary from one γ value to the next, we found that the curves are largely unchanged by partitioning the γ line into three regimes, each of which is governed by a particular configuration of the N_g gauge-invariant quantities, as reflected in the figure. Note also the relatively small difference between the 4×4 and 6×6 results.

SK found a sharp transition in the first decay modes between two regimes of dissipation strength, regardless of system size. (SK examined their model with open boundaries, but we have confirmed this result when periodic boundary conditions are applied to their model as well.) We cannot conclude whether or not this is the case for our model, but the intermediate regime we find could result from a failure of the GA to reach the block of true first decay modes. A clear intermediate regime is appar-

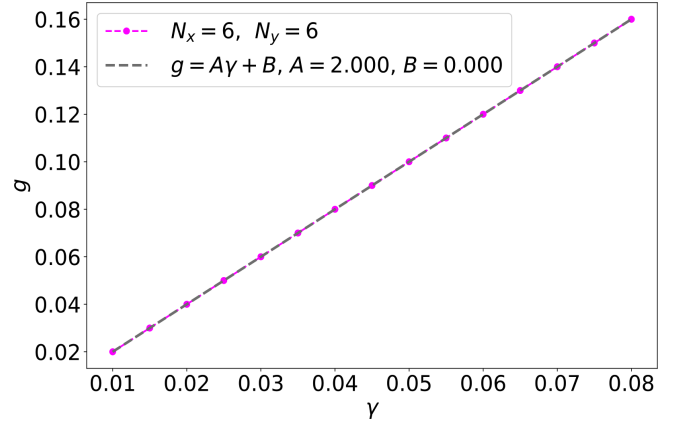


FIG. 11. Behavior at small γ for the largest system size we used in our calculations (6×6), with all $J_\delta = 1$. We obtained this curve by using the first decay modes we used to explain the small γ regime in fig. 10.

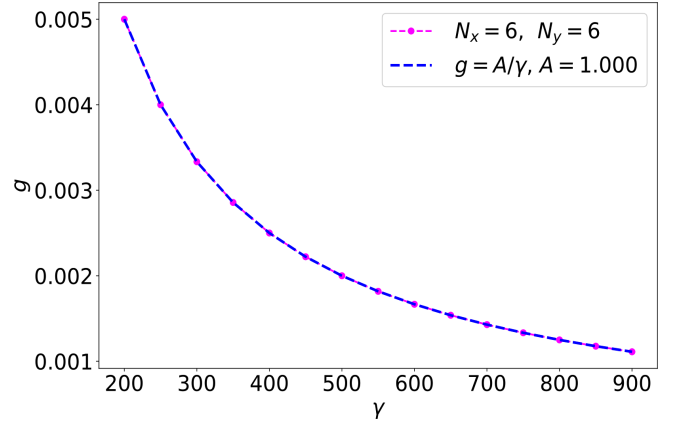


FIG. 12. Behavior at large γ for the largest system size we used in our calculations (6×6), with all $J_\delta = 1$. We obtained this curve by using the first decay modes we used to explain the large γ regime in fig. 10.

ent in the N_v -limited data of fig. 16, with all $J_\delta = 1$, for $N_v = 1, 2$ on size 4×4 . (See also fig. 17 for the case when all the J_δ are different.) For $N_v = 3, 4$ the effect is far less pronounced. Note that the $N_v = 4$ results are in good agreement with the GA results. For the 6×6 case, the $N_v = 1, 2$ results in fig. 18 are quite far from the GA curve.

From the genetic algorithm, the optimal flux configurations for the lowest nonzero decay seem to contain many defects. We list some of these configurations in the appendix §C below. For example, for the 4×4 system with all $J_\delta = 1$, the optimal excited state we obtained had 14 defects relative to the fiducial NESS with all \mathbb{Z}_2 data set to -1 . However, since we start the GA from a population of random \mathbb{Z}_2 data, it may well be that a configuration with 14 defects with respect to a particular NESS might be described by fewer defects with respect to a different state in the 2^{3N+1} -fold block of NESSes. We

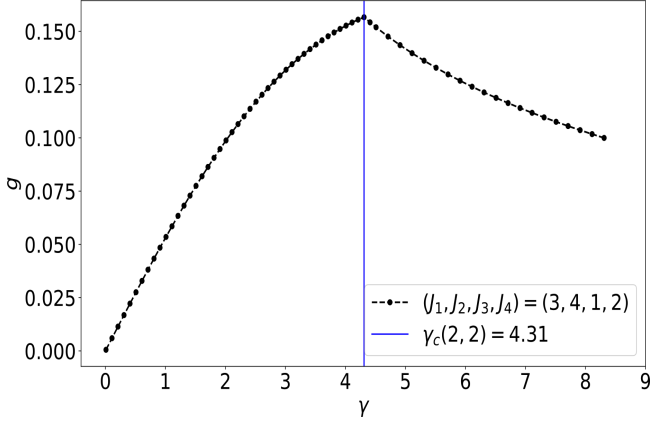


FIG. 13. Liouvillian gap for our model with periodic boundary conditions for $N_x = N_y = 2$ and $(J_1, J_2, J_3, J_4) = (3, 4, 1, 2)$: The Liouvillian gap, g , as a function of γ . There is a transition in the first decay modes at the cusp seen at $\gamma = \gamma_c(2, 2)$, depicted by the blue vertical line. We see a transition in the first decay modes. We have 2 first decay modes for $\gamma < \gamma_c(2, 2)$ and eight first decay modes for $\gamma \geq \gamma_c(2, 2)$.

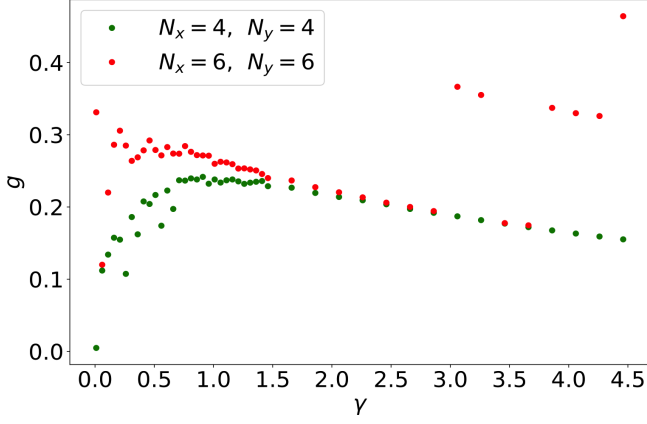


FIG. 14. Minimal relaxation rate g versus γ obtained over different runs of the genetic algorithm with $(J_1, J_2, J_3, J_4) = (3, 4, 1, 2)$ for system sizes 4×4 and 6×6 . The population size was 100 and the number of runs was 10.

are now attempting to better clarify the minimal defect content of the degenerate excited states.

We try fitting the $g(\gamma)$ curves to identify their behavior for small and large values of the dissipation strength γ (see figs. 11 and 12). The shape of the $g(\gamma)$ curves is similar to that found by Shibata and Katsura [1], rising linearly from zero at small γ and decaying as $1/\gamma$ for large γ . In the appendix §A, we provide analytical support for these behaviors.

We also investigate the behavior of the gap for the case $(J_1, J_2, J_3, J_4) = (3, 4, 1, 2)$, which breaks certain discrete translation and rotation symmetries present in the model when all J_δ are equal. The results are shown in figs. 13, 14 and 15. GA and the phases are obtained as described above. While the shape of the curves is similar, we find two significant differences. First, from fig. 15 it appears

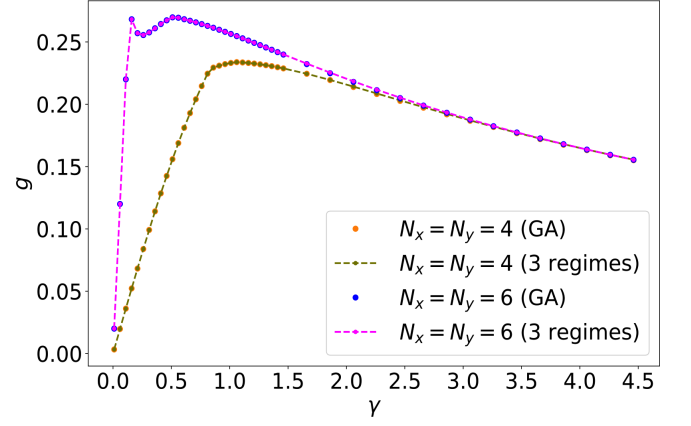


FIG. 15. GA and the phases are described in the text. Here, $(J_1, J_2, J_3, J_4) = (3, 4, 1, 2)$. The 3 regimes for 4×4 are separated by $\gamma_1^* = 0.86$ and $\gamma_2^* = 1.06$ and the three regimes for 6×6 are separated by $\gamma_1^* = 0.16$ and $\gamma_2^* = 0.51$.

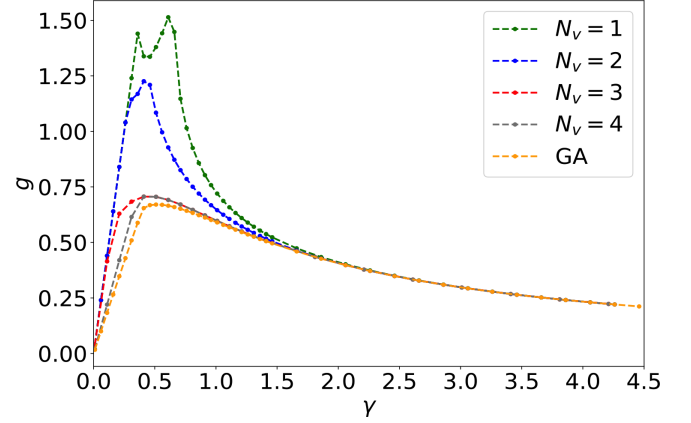


FIG. 16. The GA curve and the curves obtained by considering configurations with a given number of vortices N_v , as described in the text. Here all $J_\delta = 1$ and the system size is 4×4 .

that the GA has not found the lowest decay mode in the small γ regime, where the 4×4 and 6×6 GA results differ substantially. Second, as shown in fig. 17, the $N_v \leq 4$ sector does not yield a good approximation to the GA results, as it did for the case with all $J_\delta = 1$.

V. CONCLUSIONS

In this paper we have described a two-dimensional square lattice model of interacting gamma matrix ‘spins’ coupled to a dissipative environment. The density matrix evolution is described by the GKLS master equation $\dot{\rho} = \mathcal{L}\rho$, where \mathcal{L} is the Liouvillian, which in general has complex eigenvalues Λ_a . This description is equivalent to Schrödinger evolution under a non-Hermitian Hamiltonian \mathcal{W} on a square lattice bilayer, whose eigenvalues are $E_a = i\Lambda_a$. Our model is inspired by, and a generaliza-

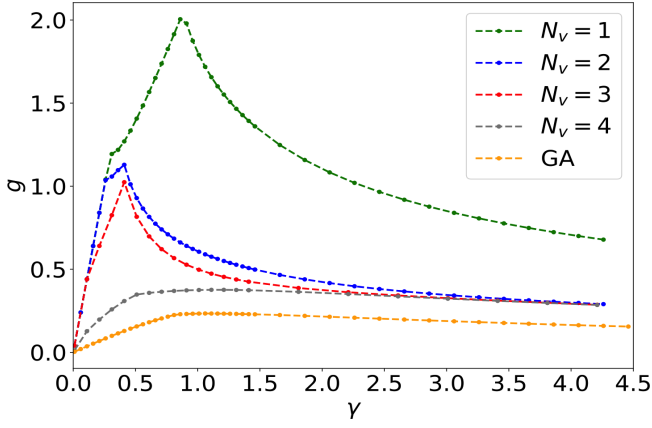


FIG. 17. The GA curve and the curves obtained by considering configurations with a given number of vortices N_v , as described in the text. Here $(J_1, J_2, J_3, J_4) = (3, 4, 1, 2)$ and the system size is 4×4 .

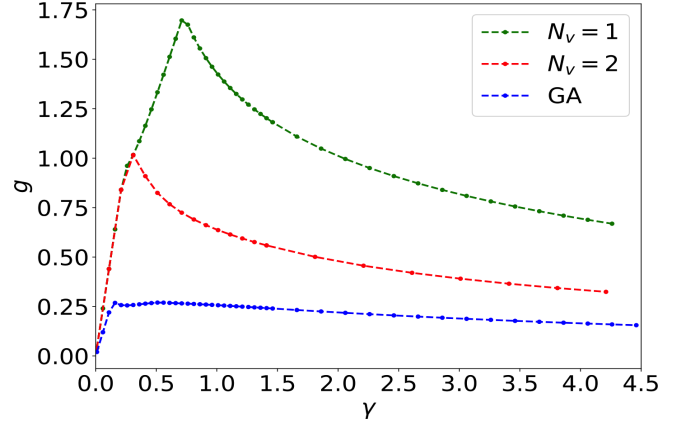


FIG. 19. The GA curve and the curves obtained by considering configurations with a given number of vortices N_v , as described in the text. Here all $(J_1, J_2, J_3, J_4) = (3, 4, 1, 2)$ and the system size is 6×6 .

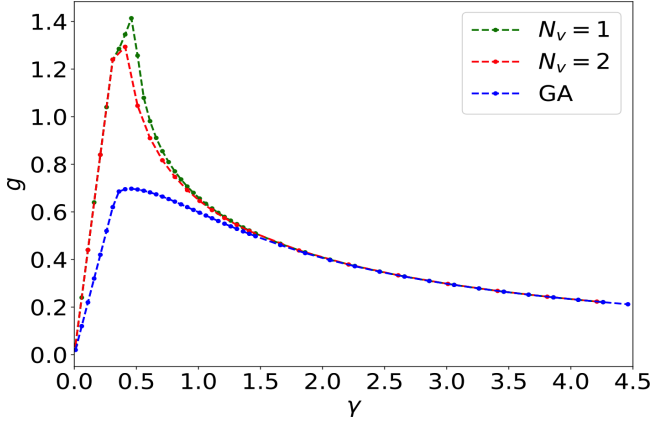


FIG. 18. The GA curve and the curves obtained by considering configurations with a given number of vortices N_v , as described in the text. Here all $J_\delta = 1$ and the system size is 6×6 .

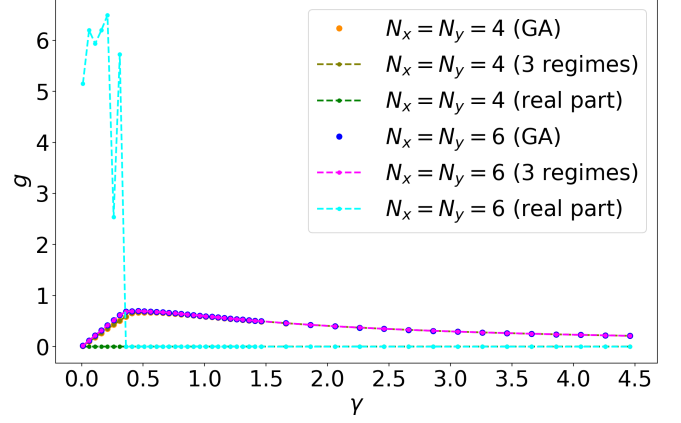


FIG. 20. Imaginary (g) and real parts of the lowest decay modes as a function of γ for 4×4 and 6×6 lattices, with $(J_1, J_2, J_3, J_4) = (1, 1, 1, 1)$. $\text{Re } E_a = 0$ in all cases except for 6×6 with $\gamma < \gamma_c$.

tion of, the dissipative one-dimensional Pauli matrix spin model of Shibata and Katsura [1]. It is in the ‘solvable’ class of models exemplified by Kitaev’s celebrated honeycomb lattice model [2], equivalent to a single species of Majorana fermion hopping in a nondynamical \mathbb{Z}_2 background gauge field. It is solvable in the sense that for any given configuration of the gauge-invariant plaquette fluxes and Wilson phases, the non-Hermitian Hamiltonian \mathcal{W} is quadratic and solvable by Prosen’s method [4]. However, there are exponentially many such configurations, and when the gauge field structure is not translationally invariant, the Hamiltonian must be diagonalized numerically. Furthermore, there is no analog of Lieb’s theorem [6] to assist us in identifying the longest lived decaying eigenmodes.

In the infinite time limit, the system approaches one of an exponentially large number of nonequilibrium steady states, with a spectrum $\{-\text{Im } E_a\}$ of relaxation rates.

The minimum relaxation rate $g(\gamma)$ is typically achieved for different \mathbb{Z}_2 flux configurations in the small and large γ limits, a feature also observed by Shibata and Katsura.

We have not indicated in our plots the spectrum $\{\text{Re } E_a\}$ of the real parts of the eigenvalues of \mathcal{W} . This is because in almost all cases studied we have found the imaginary parts of the first decay mode eigenvalues to be zero. The only exception we observed was in the 6×6 case with all J couplings equal and for $\gamma < \gamma_c$, as shown in fig. 20 [16] (When all J ’s are different, we find $\text{Re } E_a = 0$ for the lowest decay modes, for all γ and all sizes.)

Our model can further be generalized to other lattices. The Kitaev solvability of the SK model is associated with the fact that their model is equivalent to non-Hermitian Hamiltonian evolution on a two leg ladder, where each site lies at the confluence of three distinct classes of links. For the dimension k Clifford algebra, we have $2k + 1$ gamma matrices of dimension 2^k , and a Kitaev Hamilto-

nian (Hermitian or not) can be constructed on any lattice where each site lies at the confluence of $(2k+1)$ distinct classes of links [8]. Thus, for $k=2$, our square lattice bilayer is five-fold coordinated. A corresponding model could thus be constructed on the kagome lattice, leading to a non-Hermitian Dirac matrix Hamiltonian \mathcal{W} on the kagome bilayer. (Further generalizations of this construction can result in multiple species of hopping and hybridizing Majoranas in the presence of a background nondynamical gauge field, as in refs. [7, 13].) Thus, proceeding to $k=3$ with its seven 8×8 gamma matrices, a corresponding model can be constructed on a cubic lattice (bipartite NaCl structure) with $\Gamma_{\mathbf{R}}^{\delta} \Gamma_{\mathbf{R}+\delta}^{\delta}$ interactions on each class δ link with $\delta \in \{1, \dots, 6\}$ and Lindblad jump operators $\sqrt{\gamma} \Gamma_{\mathbf{r}}^{\delta}$ at each site. Again, there will be an exponentially large block of NESS density matrices owing to the conserved plaquette fluxes.

Note: Some of this work was presented in a poster at the KITP Workshop, *Topology, Symmetry and Interactions in Crystals: Emerging Concepts and Unifying Themes* (KITP UC Santa Barbara, April 3–6, 2023) [17]. While this article was in the final stages of preparation, an analysis of two largely equivalent models appeared on the arXiv [9, 10].

VI. ACKNOWLEDGEMENTS

We gratefully acknowledge conversations with Tarun Grover and John McGreevy. We thank Debanjan Chowdhury for alerting us to ref. [10]. This research was funded in part by General Campus Research Award RG104654 from the UC San Diego Academic Senate.

-
- [1] Naoyuki Shibata and Hosho Katsura. Dissipative spin chain as a non-Hermitian Kitaev Ladder. *Physical review B*, 99(17):174303, 2019.
 - [2] Naoyuki Shibata and Hosho Katsura. Anyons in an exactly solved model and beyond. *Annals of Physics*, 321(1):2, 2006.
 - [3] Heinz-Peter Breuer and Francesco Petruccione. *The Theory of Open Quantum Systems*. Oxford University Press, 01 2007.
 - [4] Third quantization: a general method to solve master equations for quadratic open Fermi systems. *New Journal of Physics*, 10(4):043026, apr 2008.
 - [5] Dariusz Chruściński and Saverio Pascazio. A Brief History of the GKLS Equation. *Open Systems and Information Dynamics*, 24(03):1740001, sep 2017.
 - [6] Elliott H. Lieb. Two theorems on the Hubbard model. *Phys. Rev. Lett.*, 62:1201–1204, Mar 1989.
 - [7] Hong Yao, Shou-Cheng Zhang, and Steven A. Kivelson. Algebraic Spin Liquid in an Exactly Solvable Spin Model. *Phys. Rev. Lett.*, 102:217202, May 2009.
 - [8] Congjun Wu, Daniel Arovas, and Hsiang-Hsuan Hung. Γ -matrix generalization of the Kitaev model. *Physical review B*, 79(13):134427, 2009.
 - [9] Xu-Dong Dai, Fei Song, and Zhong Wang. Solvable BCS-Hubbard Lindbladians in arbitrary dimensions. arXiv 2306.13148.
 - [10] Henry Shackleton and Mathias S. Scheurer. An exactly solvable dissipative spin liquid. arXiv 2307.05743.
 - [11] Victor V. Albert. Lindbladians with multiple steady states: theory and applications. arXiv 1802.00010.
 - [12] Alan A Dzhioev and D S Kosov. Nonequilibrium perturbation theory in liouville–fock space for inelastic electron transport. *Journal of Physics: Condensed Matter*, 24(22):225304, may 2012.
 - [13] Victor Chua, Hong Yao, and Gregory A. Fiete. Exact chiral spin liquid with stable spin Fermi surface on the kagome lattice. *Phys. Rev. B*, 83:180412, May 2011.
 - [14] We find it convenient here to use expressions $\Gamma^{\mu\nu} \equiv -\Gamma^{\nu\mu}$ with $\mu > \nu$.
 - [15] There is of course a single remaining constraint associated with the condition $\text{Tr } \rho = 1$.
 - [16] Modes with equal and opposite nonzero values of E_a are degenerate. We cannot rule out the possibility that there are degenerate lowest decay modes for the 6×6 lattice with uniform J_{δ} with $\text{Re } E_a = 0$.
 - [17] Jyotsna Gidugu and Daniel P. Arovas. A study on dissipative models based on Γ -matrices. https://online.kitp.ucsb.edu/online/qcrystal-c23/gidugu/qcrystal-c23_poster_gidugu.pdf, 2023.
 - [18] Tankut Can, Vadim Oganesyan, Dror Orgad, and Sarang Gopalakrishnan. Spectral gaps and midgap states in random quantum master equations. *Phys. Rev. Lett.*, 123:234103, Dec 2019.
 - [19] Roger A. Horn and Charles R. Johnson. *Matrix Analysis*. Cambridge University Press, 1985.

Appendix A: Perturbation Theory for Large and Small values of γ

Can *et al.* [18] considered a model of a random Hermitian Hamiltonian H in the presence of a single Hermitian jump operator $\sqrt{\gamma} L$, with both H and L random and chosen from the Gaussian unitary ensemble. They showed how the spectrum of relaxation times could be computed perturbatively in the small and large γ limits, by perturbing in the dissipator $\mathcal{L}_D = \frac{1}{2}\gamma[L, [\bullet, L]]$ or in the non-dissipative Liouvillian $\mathcal{L}_H = -i[H, \bullet]$, respectively. Thus, at small γ , the smallest nonzero relaxation rate τ^{-1} is proportional to γ , while at large γ it is proportional to γ^{-1} . In this appendix we perform a related analysis for our model.

1. $\gamma \ll 1$

For $\gamma \ll 1$ we write the GKLS equation as a classical master equation for the projectors $P_\alpha = |\alpha\rangle\langle\alpha|$, where α is an eigenstate of the Hamiltonian H [18]. This classical master equation is written

$$\frac{dP_\alpha}{dt} = \gamma \mathcal{M}_{\alpha\beta} P_\beta \quad , \quad (\text{A1})$$

with

$$\mathcal{M}_{\alpha\beta} = \sum_{\mathbf{r}} \left(|\langle\alpha|\Gamma_{\mathbf{r}}^5|\beta\rangle|^2 - \delta_{\alpha\beta} \right) \quad . \quad (\text{A2})$$

Clearly this analysis will lead in this limit to real eigenvalues proportional to γ . What is the coefficient for the smallest such eigenvalue?

To analyze this, we start with our Hamiltonian,

$$H = i \sum_{\mathbf{R} \in \mathbf{A}} \sum_{\delta=1}^4 J_\delta u_{\mathbf{R}}^\delta \theta_{\mathbf{R}}^0 \theta_{\mathbf{R}+\delta}^0 \equiv \frac{i}{2} \sum_{\mathbf{r}, \mathbf{r}'} J_{\mathbf{r}, \mathbf{r}'} \theta_{\mathbf{r}}^0 \theta_{\mathbf{r}'}^0 \quad , \quad (\text{A3})$$

where $J_{\mathbf{r}, \mathbf{r}'}$ is a real antisymmetric matrix with $J_{\mathbf{R}, \mathbf{R}+\delta} = J^\delta u_{\mathbf{R}}^\delta$. The $\theta_{\mathbf{r}}^5$ Majoranas are cyclic in H and lead to an exponential degeneracy $\sim 2^{N_c}$ for each energy level. Including the $N-1$ plaquette fluxes and the two Wilson phases, and accounting for the constraint

$$\prod_{\mathbf{r}} i \theta_{\mathbf{r}}^0 \theta_{\mathbf{r}}^1 \theta_{\mathbf{r}}^2 \theta_{\mathbf{r}}^3 \theta_{\mathbf{r}}^4 \theta_{\mathbf{r}}^5 = 1 \quad , \quad (\text{A4})$$

which constrains the combined parity of the $a=0$ and $a=5$ species fermions given the gauge fields $u_{\mathbf{r}, \mathbf{r}'}$, we have a total of 4^N projectors: 2^{N+1} from plaquette fluxes and Wilson phases (see Fig. 5), and 2^{N-1} for the parity-constrained $a=0, 5$ fermions. This is a subset of the 16^N (unnormalized) density matrices.

Every real antisymmetric matrix can be diagonalized by an orthogonal transformation. For each gauge field configuration, the corresponding real antisymmetric matrix $J_{\mathbf{r}, \mathbf{r}'}$ is brought to block diagonal form by a real orthogonal matrix $Q_{\mathbf{r}, \mathbf{s}}$, such that

$$Q^\top J Q = \text{diag} \left\{ \begin{pmatrix} 0 & \varepsilon_1 \\ -\varepsilon_1 & 0 \end{pmatrix}, \dots, \begin{pmatrix} 0 & \varepsilon_{N_c} \\ -\varepsilon_{N_c} & 0 \end{pmatrix} \right\} \quad , \quad (\text{A5})$$

where $\{\varepsilon_{\mathbf{S}}\}$ are the singular values of J [19]. We define a new set of Majoranas $\xi_{\mathbf{s}} = \theta_{\mathbf{r}}^0 Q_{\mathbf{r}, \mathbf{s}}$, and we may associate each \mathbf{s} with a site on the $N_x \times N_y$ square lattice, exactly as is the case for the \mathbf{r} sites. Thus, the \mathbf{s} values are divided into A and B sublattices, and writing $\mathbf{S} \in \mathbf{A}$ we have $\mathbf{S} + \hat{\mathbf{x}} \in \mathbf{B}$. Each of the 2×2 blocks in eqn. A5 is then associated with $\mathbf{s} = \mathbf{S}$ and $\mathbf{s}' = \mathbf{S} + \hat{\mathbf{x}}$, for some \mathbf{S} . We now define

$$c_{\mathbf{S}} = \frac{1}{2}(\xi_{\mathbf{S}} - i\xi_{\mathbf{S}+\hat{\mathbf{x}}}) \quad , \quad c_{\mathbf{S}}^\dagger = \frac{1}{2}(\xi_{\mathbf{S}} + i\xi_{\mathbf{S}+\hat{\mathbf{x}}}) \quad , \quad d_{\mathbf{R}} = \frac{1}{2}(\theta_{\mathbf{R}}^5 - i\theta_{\mathbf{R}+\hat{\mathbf{x}}}^5) \quad , \quad d_{\mathbf{R}}^\dagger = \frac{1}{2}(\theta_{\mathbf{R}}^5 + i\theta_{\mathbf{R}+\hat{\mathbf{x}}}^5) \quad , \quad (\text{A6})$$

which entail

$$\xi_{\mathbf{S}} = c_{\mathbf{S}}^\dagger + c_{\mathbf{S}} \quad , \quad \xi_{\mathbf{S}+\hat{\mathbf{x}}} = i(c_{\mathbf{S}}^\dagger - c_{\mathbf{S}}) \quad , \quad \theta_{\mathbf{R}}^5 = d_{\mathbf{R}}^\dagger + d_{\mathbf{R}} \quad , \quad \theta_{\mathbf{R}+\hat{\mathbf{x}}}^5 = i(d_{\mathbf{R}}^\dagger - d_{\mathbf{R}}) \quad . \quad (\text{A7})$$

The Hamiltonian is then $H = \sum_{\mathbf{S}} \varepsilon_{\mathbf{S}} (2c_{\mathbf{S}}^\dagger c_{\mathbf{S}} - 1)$. We may now write

$$\begin{aligned} \Gamma_{\mathbf{R}}^5 &= \sum_{\mathbf{S}} \left\{ i Q_{\mathbf{S}, \mathbf{R}}^{\text{AA}} (c_{\mathbf{S}}^\dagger + c_{\mathbf{S}})(d_{\mathbf{R}}^\dagger + d_{\mathbf{R}}) + Q_{\mathbf{S}, \mathbf{R}}^{\text{BA}} (c_{\mathbf{S}} - c_{\mathbf{S}}^\dagger)(d_{\mathbf{R}}^\dagger + d_{\mathbf{R}}) \right\} \\ \Gamma_{\mathbf{R}+\hat{\mathbf{x}}}^5 &= \sum_{\mathbf{S}} \left\{ Q_{\mathbf{S}, \mathbf{R}}^{\text{AB}} (c_{\mathbf{S}}^\dagger + c_{\mathbf{S}})(d_{\mathbf{R}} - d_{\mathbf{R}}^\dagger) - i Q_{\mathbf{S}, \mathbf{R}}^{\text{BB}} (c_{\mathbf{S}} - c_{\mathbf{S}}^\dagger)(d_{\mathbf{R}} - d_{\mathbf{R}}^\dagger) \right\} \quad , \end{aligned} \quad (\text{A8})$$

where

$$Q_{\mathbf{S}, \mathbf{R}}^{\text{AA}} = Q_{\mathbf{S}, \mathbf{R}} \quad , \quad Q_{\mathbf{S}, \mathbf{R}}^{\text{AB}} = Q_{\mathbf{S}, \mathbf{R}+\hat{\mathbf{x}}} \quad , \quad Q_{\mathbf{S}, \mathbf{R}}^{\text{BA}} = Q_{\mathbf{S}+\hat{\mathbf{x}}, \mathbf{R}} \quad , \quad Q_{\mathbf{S}, \mathbf{R}}^{\text{BB}} = Q_{\mathbf{S}+\hat{\mathbf{x}}, \mathbf{R}+\hat{\mathbf{x}}} \quad . \quad (\text{A9})$$

Now consider the matrix elements $\langle \mathbf{m}, \mathbf{n} | \Gamma_{\mathbf{R}}^5 | \mathbf{m}', \mathbf{n}' \rangle$ and $\langle \mathbf{m}, \mathbf{n} | \Gamma_{\mathbf{R}+\hat{x}}^5 | \mathbf{m}', \mathbf{n}' \rangle$, where

$$|\mathbf{m}, \mathbf{n}\rangle \equiv \prod_{\mathbf{S}} (c_{\mathbf{S}}^\dagger)^{m_{\mathbf{S}}} \prod_{\mathbf{R}} (d_{\mathbf{R}}^\dagger)^{n_{\mathbf{R}}} |0\rangle, \quad (\text{A10})$$

where $|0\rangle$ is the vacuum for c and d fermions. Then

$$\sum_{\mathbf{r}} |\langle \mathbf{m}, \mathbf{n} | \Gamma_{\mathbf{r}}^5 | \mathbf{m}', \mathbf{n}' \rangle|^2 = \sum_{\mathbf{R}_1} \sum_{\mathbf{S}_1} \left[(Q_{\mathbf{S}_1, \mathbf{R}_1}^{\text{AA}})^2 + (Q_{\mathbf{S}_1, \mathbf{R}_1}^{\text{AB}})^2 + (Q_{\mathbf{S}_1, \mathbf{R}_1}^{\text{BA}})^2 + (Q_{\mathbf{S}_1, \mathbf{R}_1}^{\text{BB}})^2 \right] \tilde{\delta}_{\mathbf{m}, \mathbf{m}', \mathbf{S}_1} \tilde{\delta}_{\mathbf{n}, \mathbf{n}', \mathbf{R}_1}, \quad (\text{A11})$$

where we have defined the symbol

$$\tilde{\delta}_{\mathbf{m}, \mathbf{m}', \mathbf{S}_1} = \delta_{m'_{\mathbf{S}_1}, 1-m_{\mathbf{S}_1}} \times \prod_{\mathbf{S} \neq \mathbf{S}_1} \delta_{m'_{\mathbf{S}}, m_{\mathbf{S}}} \quad (\text{A12})$$

In other words, $\tilde{\delta}_{\mathbf{m}, \mathbf{m}', \mathbf{S}_1} = 1$ when $m_{\mathbf{S}} = m'_{\mathbf{S}}$ for all \mathbf{S} other than \mathbf{S}_1 , where the two occupations are complementary.

When the gauge fields have the periodicity of the lattice, *i.e.* when $u_{\mathbf{R}}^\delta = u_{\mathbf{R}'}^\delta$ for all \mathbf{R} and \mathbf{R}' , translational invariance allows us to simplify eqn. A11, in which case

$$\mathcal{M}_{\mathbf{m}\mathbf{n}, \mathbf{m}'\mathbf{n}'} = \frac{4}{N} \delta_{d(\mathbf{m}, \mathbf{m}'), 1} \delta_{d(\mathbf{n}, \mathbf{n}'), 1} - N \delta_{\mathbf{m}, \mathbf{m}'} \delta_{\mathbf{n}, \mathbf{n}'}, \quad (\text{A13})$$

where $d(\mathbf{m}, \mathbf{m}')$ is the number of locations where the occupation $\mathbf{m}_{\mathbf{s}}$ differs from $\mathbf{m}'_{\mathbf{s}}$. The eigenvalues of \mathcal{M} are then given by

$$\Lambda(\boldsymbol{\sigma}, \boldsymbol{\mu}) = \frac{4}{N} (\sigma_1 + \dots + \sigma_{N_c}) (\mu_1 + \dots + \mu_{N_c}) - N, \quad (\text{A14})$$

where each $\sigma_{\mathbf{S}}$ and $\mu_{\mathbf{R}}$ are either 0 or 1. When all $\sigma_{\mathbf{S}}$ and $\mu_{\mathbf{R}}$ are +1 or all are -1, the eigenvalue is zero, corresponding to a NESS. When one of the σ or μ values has a reversed sign, we obtain $\Lambda = -2$, corresponding to a Liouvillian eigenvalue of -2γ . Numerically, we find that the slope of the smallest nonzero decay rate $-\text{Re } \Lambda(\gamma)$ is 1 rather than 2. It may be that for sectors of \mathcal{M} corresponding to non-translationally invariant flux configurations, where the Q -matrices don't reflect such a symmetry, that the coefficient for the lowest decay rate is smaller, but we do not understand how to arrive at a slope of 1. Another possibility we have not explored is the dynamics of a restricted class of coherences $|\alpha\rangle\langle\beta|$, where $|\alpha\rangle = |\mathbf{m}, \mathbf{n}_1\rangle$ and $|\beta\rangle = |\mathbf{m}, \mathbf{n}_2\rangle$. There are $2^{5N/2}$ such coherences, all of which commute with H , arranged into 2^N blocks of size $2^{3N/2}$. The generalization of the matrix \mathcal{M} in each block is then

$$\mathcal{M}_{\mathbf{m}, \mathbf{n}_1, \mathbf{n}_2, \mathbf{m}', \mathbf{n}'_1, \mathbf{n}'_2} = \sum_{\mathbf{r}} \sum_{\mathbf{M}} \sum_{\mathbf{N}_1} \sum_{\mathbf{N}_2} \left(\langle \mathbf{M}, \mathbf{N}_1 | \Gamma_{\mathbf{r}}^5 | \mathbf{n}, \mathbf{n}_1 \rangle \langle \mathbf{m}, \mathbf{n}_2 | \Gamma_{\mathbf{r}}^5 | \mathbf{M}, \mathbf{N}_2 \rangle - \delta_{\mathbf{M}, \mathbf{m}} \delta_{\mathbf{M}_1, \mathbf{n}_1} \delta_{\mathbf{M}_2, \mathbf{n}_2} \right). \quad (\text{A15})$$

While the the matrix element products

$$\langle \mathbf{N}_1 | d_{\mathbf{R}}^\dagger \pm d_{\mathbf{R}} | \mathbf{n}_1 \rangle \langle \mathbf{n}_2 | d_{\mathbf{R}}^\dagger \pm d_{\mathbf{R}} | \mathbf{N}_2 \rangle \quad (\text{A16})$$

are nonzero only if \mathbf{N}_1 and \mathbf{n}_1 have complementary occupancies in the same location \mathbf{R} as do \mathbf{N}_2 and \mathbf{n}_2 , the presence of occupation number dependent sign factors complicates the analysis.

2. $\gamma \gg 1$

We start with the Dirac matrices,

$$\begin{aligned} \Gamma^1 &= X \otimes 1 = \begin{pmatrix} 0 & 0 & 1 & 0 \\ 0 & 0 & 0 & 1 \\ 1 & 0 & 0 & 0 \\ 0 & 1 & 0 & 0 \end{pmatrix} & \Gamma^2 &= Y \otimes 1 = \begin{pmatrix} 0 & 0 & -i & 0 \\ 0 & 0 & 0 & -i \\ i & 0 & 0 & 0 \\ 0 & i & 0 & 0 \end{pmatrix} & \Gamma^3 &= Z \otimes X = \begin{pmatrix} 0 & 1 & 0 & 0 \\ 1 & 0 & 0 & 0 \\ 0 & 0 & 0 & -1 \\ 0 & 0 & -1 & 0 \end{pmatrix} \\ \Gamma^4 &= Z \otimes Y = \begin{pmatrix} 0 & -i & 0 & 0 \\ i & 0 & 0 & 0 \\ 0 & 0 & 0 & -i \\ 0 & 0 & i & 0 \end{pmatrix} & \Gamma^5 &= Z \otimes Z = \begin{pmatrix} 1 & 0 & 0 & 0 \\ 0 & -1 & 0 & 0 \\ 0 & 0 & -1 & 0 \\ 0 & 0 & 0 & 1 \end{pmatrix}. \end{aligned} \quad (\text{A17})$$

We label the eigenstates of Γ^5 by an index $\mu \in \{1, 2, 3, 4\}$, with eigenvectors $\psi_i^{(\mu)} = \delta_{i,\mu}$ and with eigenvalues $\zeta_\mu = \{1, -1, -1, 1\}$, respectively. Since $\mathcal{L}_D \varrho = \gamma \sum_{\mathbf{r}} (\Gamma_{\mathbf{r}}^5 \varrho \Gamma_{\mathbf{r}}^5 - \varrho)$, any operator $|\mu\rangle\langle\nu|$ is annihilated by \mathcal{L}_D provided it is an eigenoperator under the action of $\Gamma_{\mathbf{r}}^5$ from either the left or the right, at every site \mathbf{r} . There are 8^N such operators, since we can freely choose each of the $\mu_{\mathbf{r}}$ so long as $\nu_{\mathbf{r}} = \mu_{\mathbf{r}}$ or $\nu_{\mathbf{r}} = 5 - \mu_{\mathbf{r}}$. In general, the eigenoperators of \mathcal{L}_D are arranged into sectors Υ_k , where $|\mu\rangle\langle\nu| \in \Upsilon_k$ provided $\zeta_{\mu_{\mathbf{r}}} \neq \zeta_{\nu_{\mathbf{r}}}$ at k locations \mathbf{r} . The eigenvalue under \mathcal{L}_D for any operator in sector Υ_k is then $-2k\gamma$.

We label the 8^N operators in the Υ_0 sector as $A_{\mathbf{p}} = |\mu\rangle\langle\nu|$, with $p_{\mathbf{r}} = \mu_{\mathbf{r}}$ if $\nu_{\mathbf{r}} = \mu_{\mathbf{r}}$ and $p_{\mathbf{r}} = \mu_{\mathbf{r}} + 4$ if $\nu_{\mathbf{r}} = 5 - \mu_{\mathbf{r}}$ at each site \mathbf{r} . We also define the $N \cdot 8^N$ operators

$$B_{\mathbf{p}}^l = i |\mu\rangle\langle\nu| H_l - i H_l |\mu\rangle\langle\nu| \quad , \quad (\text{A18})$$

where l denotes one of the $2N$ links $(\mathbf{R}, \mathbf{R} + \delta)$ and where $H_l = J_\delta \Gamma_{\mathbf{R}}^\delta \Gamma_{\mathbf{R}+\delta}^\delta$. For simplicity we shall assume $J_\delta = 1$ for each of the four types of links, although our method described below can easily be applied to the more general case. Since each of the matrices $\Gamma^{1,2,3,4}$ anticommutes with Γ^5 , its application reverses the Γ^5 eigenvalue, and thus $B_{\mathbf{p}}^l \in S_2$ for all \mathbf{p} and links l . We then have

$$\mathcal{L}_H A_{\mathbf{p}} = \sum_l B_{\mathbf{p}}^l \quad . \quad (\text{A19})$$

We wish to analyze the Liouvillian $\mathcal{L} = \mathcal{L}_H + \mathcal{L}_D$ when restricted to the subspace $S_0 \cup S'_2$, where $S'_2 \subset S_2$ includes operators $|\mu\rangle\langle\nu|$ where there are differences in the Γ^5 eigenvalues of the bra and ket states at two sites from the same link. In other words, we restrict the action of \mathcal{L} to the subspace of operators spanned by the $A_{\mathbf{p}}$ and the $B_{\mathbf{p}}^l$. The total dimension of this operator space is then $(2N + 1) \cdot 8^N$, since there are $2N$ values of l .

We now need to evaluate $\mathcal{L}_H B_{\mathbf{p}}^l$. We have

$$\mathcal{L}_H B_{\mathbf{p}}^l = 2 A_{\mathbf{p}}^l - 2 A_{\mathbf{p}} + \dots \quad , \quad (\text{A20})$$

where $A_{\mathbf{p}}^l \equiv H_l |\mu\rangle\langle\nu| H_l$, which also this lives in sector S_0 provided $|\mu\rangle\langle\nu| \in S_0$. The remaining terms include operators in other sectors $S_{k>2}$ and operators in S_2 where the differences in the $\Gamma_{\mathbf{r}}^5$ eigenvalues of the bra and ket states are at two sites not connected by a link, thus requiring two applications of \mathcal{L}_H to reach from S_0 . In this basis, the matrix form of the projected Liouvillian $\tilde{\mathcal{L}}$ is

$$\tilde{\mathcal{L}} = \begin{pmatrix} 0 & -2R_1 & -2R_2 & \cdots & -2R_M \\ 1 & -4\gamma\mathbb{1} & 0 & & 0 \\ 1 & 0 & -4\gamma\mathbb{1} & & 0 \\ \vdots & & & \ddots & \vdots \\ 1 & 0 & \cdots & & -4\gamma\mathbb{1} \end{pmatrix} \Rightarrow \omega - \tilde{\mathcal{L}} = \begin{pmatrix} \omega\mathbb{1} & 2R_1 & 2R_2 & \cdots & 2R_M \\ -1 & (\omega + 4\gamma)\mathbb{1} & 0 & & 0 \\ -1 & 0 & (\omega + 4\gamma)\mathbb{1} & & 0 \\ \vdots & & & \ddots & \vdots \\ -1 & 0 & \cdots & & (\omega + 4\gamma)\mathbb{1} \end{pmatrix} \quad , \quad (\text{A21})$$

where $M = 2N$ is the number of links in the square lattice (with periodic boundary conditions.) We can now perform row and column reduction on the matrix $\omega - \tilde{\mathcal{L}}$ to obtain

$$\omega - \tilde{\mathcal{L}} \mapsto \begin{pmatrix} \omega & 2\mathcal{S}_M & 2\mathcal{S}_{M-1} & \cdots & 2\mathcal{S}_1 \\ -1 & (\omega + 4\gamma)\mathbb{1} & 0 & & 0 \\ 0 & 0 & (\omega + 4\gamma)\mathbb{1} & & 0 \\ 0 & 0 & 0 & & 0 \\ \vdots & & & \ddots & \vdots \\ 0 & \cdots & & (\omega + 4\gamma)\mathbb{1} & 0 \\ & & & 0 & (\omega + 4\gamma)\mathbb{1} \end{pmatrix} \quad , \quad (\text{A22})$$

where $\mathcal{S}_k = \sum_{l=1}^k R_l$, and the characteristic polynomial is

$$P(\omega) = (\omega + 4\gamma)^{(M-1)D} \det(\omega^2 + 4\gamma\omega + 2\mathcal{S}) \quad , \quad (\text{A23})$$

where $D = 8^N$ and where we define $\mathcal{S} \equiv \mathcal{S}_M$. Thus there are $(M - 1)D$ degenerate eigenvalues with $\omega = -4\gamma$ and $2D$ eigenvalues

$$\omega_{j,\pm} = -2\gamma \pm \sqrt{4\gamma^2 - 2s_j} \quad , \quad (\text{A24})$$

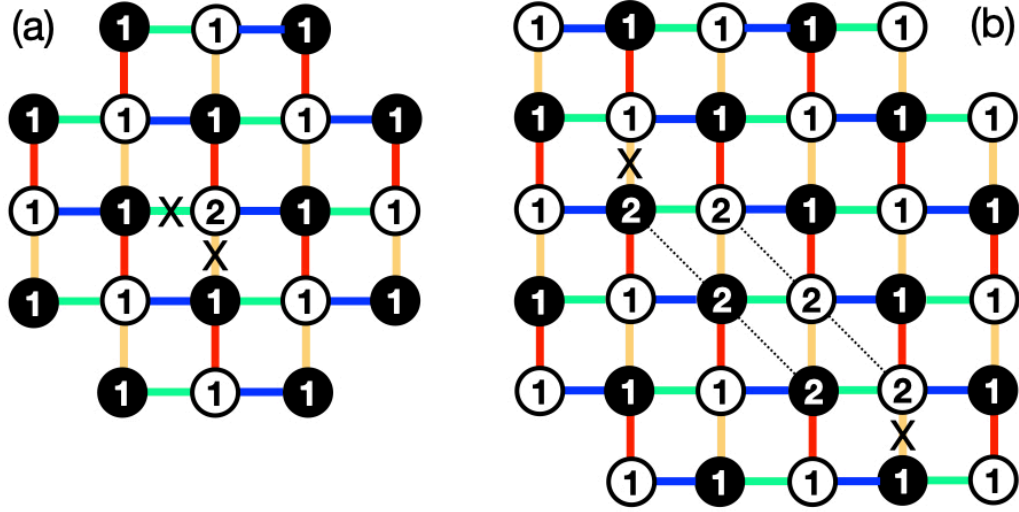


FIG. 21. Finite lifetime modes of the Liouvillian \mathcal{L} , with sites labeled by their q_r labels. (a) A configuration with $s = 4$, and (b) a string defect with $s = 4$. In both cases, $\omega = -2/\gamma$ as $\gamma \rightarrow \infty$ is the relaxation rate.

where $\{s_j\}$ are the D eigenvalues of the matrix \mathcal{S} . In the limit $\gamma \gg s_j$ we then have $\omega_{-,j} = -s_j/2\gamma + \mathcal{O}(\gamma^{-2})$. *Note:* Regarding the row and column reduction of $\omega - \tilde{\mathcal{L}}$, starting with the expression for $\omega - \tilde{\mathcal{L}}$ in eqn. A21, subtract the penultimate (M^{th}) block row from the final $((M+1)^{\text{th}})$ one. Then add the last block column from the penultimate block column. These two operations have the effect of eliminating the leftmost -1 block in the $(M+1)^{\text{th}}$ block row and replacing R_{M-1} with $R_{M-1} + R_M$ at the top of the M^{th} block column. Iterate this process until obtaining the matrix in eqn. A22.

To find the spectrum of \mathcal{S} , we note that

$$\mathcal{S}(p' | p) = M\delta_{\mu\mu'}\delta_{\nu\nu'} - \sum_{l=1}^M \langle \mu' | H_l | \mu \rangle \langle \nu | H_l | \nu' \rangle, \quad (\text{A25})$$

where each $p_r = p(\mu_r, \nu_r) \in \{1, \dots, 8\}$ is a composite index, as described above. We find

$$\Gamma^\delta A_p \Gamma^\delta = \sum_{p'} \Delta_{p,p'}^\delta A_{p'} \quad (\text{A26})$$

with

$$\Delta^{1,2} = \Gamma^1 \oplus \pm \Gamma^1, \quad \Delta^{3,4} = \Gamma^{54} \oplus \mp \Gamma^{54}. \quad (\text{A27})$$

For example,

$$\begin{aligned} \Gamma^1 A_1 \Gamma^1 &= \Gamma^1 |1\rangle \langle 1| \Gamma^1 = +|3\rangle \langle 3| = +A_3 \\ \Gamma^2 A_5 \Gamma^2 &= \Gamma^2 |1\rangle \langle 4| \Gamma^2 = -|3\rangle \langle 2| = +A_7 \\ \Gamma^3 A_6 \Gamma^3 &= \Gamma^3 |2\rangle \langle 3| \Gamma^3 = -|1\rangle \langle 4| = -A_5 \\ \Gamma^4 A_3 \Gamma^4 &= \Gamma^4 |3\rangle \langle 3| \Gamma^4 = +|4\rangle \langle 4| = -A_4. \end{aligned} \quad (\text{A28})$$

Note that $\Gamma^{54} = 1 \otimes X$. Since Γ^1 and Γ^{54} commute, we may find a common basis:

$$\vec{\varphi}_1 = \begin{pmatrix} 1 \\ 1 \\ 1 \\ 1 \end{pmatrix}, \quad \vec{\varphi}_2 = \begin{pmatrix} 1 \\ -1 \\ 1 \\ -1 \end{pmatrix}, \quad \vec{\varphi}_3 = \begin{pmatrix} 1 \\ 1 \\ -1 \\ -1 \end{pmatrix}, \quad \vec{\varphi}_4 = \begin{pmatrix} 1 \\ -1 \\ -1 \\ 1 \end{pmatrix}. \quad (\text{A29})$$

In this basis, we have

$$\begin{aligned}
\tilde{\Delta}^1 &= \text{diag}(+, +, -, -, +, +, -, -) \\
\tilde{\Delta}^2 &= \text{diag}(+, +, -, -, -, -, +, +) \\
\tilde{\Delta}^3 &= \text{diag}(+, -, +, -, -, +, -, +) \\
\tilde{\Delta}^4 &= \text{diag}(+, -, +, -, +, -, +, -) \quad .
\end{aligned} \tag{A30}$$

The eigenvalues of \mathcal{S} are thus given by

$$s(q_1, \dots, q_M) = \sum_{\mathbf{R}} \sum_{\delta=1}^4 \left(1 - \tilde{\Delta}^\delta(q_{\mathbf{R}}) \tilde{\Delta}^\delta(q_{\mathbf{R}+\delta}) \right) \quad , \tag{A31}$$

where each $q_{\mathbf{r}} \in \{1, \dots, 8\}$ and the values $\tilde{\Delta}^\delta(q)$ are given in eqn. A30. The q values label the linear combinations of single-site density matrices associated with the eight common eigenvectors of the matrices Δ^δ , *i.e.* $\begin{pmatrix} \varphi_\eta \\ \pm \varphi_\eta \end{pmatrix}$, with index $\eta \in \{1, 2, 3, 4\}$.

Clearly any configuration with all $q_{\mathbf{r}}$ equal will be a NESS, with \mathcal{S} eigenvalue $s = 0$. In fig. 21 we sketch the configurations for two excited (*i.e.* decaying) modes, with nonzero eigenvalues of \mathcal{S} . Panel (a) depicts a configuration with a single site defect, an isolated $q = 2$ state in a sea of $q = 1$. According to the rules derived here, configuration (a) has ‘bad’ bonds (labeled with an X) for which $\tilde{\Delta}^\delta(q) \tilde{\Delta}^\delta(q') = -1$, resulting in an eigenvalue $s = 4$. For configuration (b), which features two parallel diagonal line defects, there are also two bad bonds, but with a string connecting them, again giving $s = 4$. Both these configurations are highly degenerate. In the case of open boundary conditions, the string can run to a boundary, and one has a defect state with $s = 2$. Numerically, though, we find $s = 2$ to be the lowest eigenvalue of \mathcal{S} even with periodic boundary conditions.

In summary, we have analytical arguments for $\omega \propto \gamma$ as $\gamma \rightarrow 0$ and $\omega \propto \gamma^{-1}$ as $\gamma \rightarrow \infty$ based on perturbation theory, but the analytical value of the coefficient is twice that obtained from the numerical analysis.

Appendix B: Computational Procedure

The genetic algorithm that we use to estimate the was as follows. For a given gauge field configuration $F = \{\{u_{\mathbf{R}}^\delta\}, \{u_{\mathbf{r}}^5\}\}$ we find the smallest relaxation rate gap g_F by solving for the spectrum of \mathcal{W} using Prosen’s method [4]. In the genetic algorithm, the fitness function is given by the gap g_F and we try to further minimize this by varying over F . We start with a population of randomly chosen individuals (field configurations). We find individuals with low values of gap perform crossovers and mutate by flipping the sign at some places. We then calculate the gaps for the individuals in the new population and repeat the same process.

We do this over different runs, *i.e.* by starting with different randomly chosen initial populations. We pick the minimum g value obtained over different runs to be the estimate of the gap. The values over different runs for a particular value of γ are shown in figures 22 and 23 for different values of J_1, J_2, J_3 and J_4 .

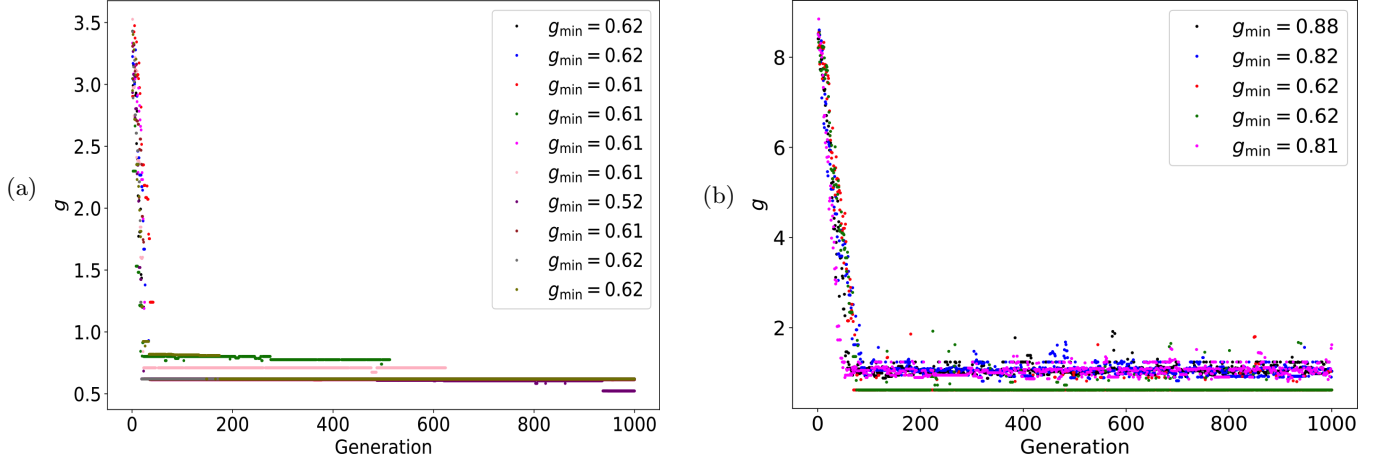


FIG. 22. Different runs of the genetic algorithm. Each color depicts a run with a randomly chosen initial population for $\gamma = 0.31$ and all $J_\delta = 1$ for different system sizes: (a) $N_x = N_y = 4$, population size 100. (b) $N_x = N_y = 6$, population size 100. In these plots, g_{\min} refers to the minimum value of the gap encountered in the run.

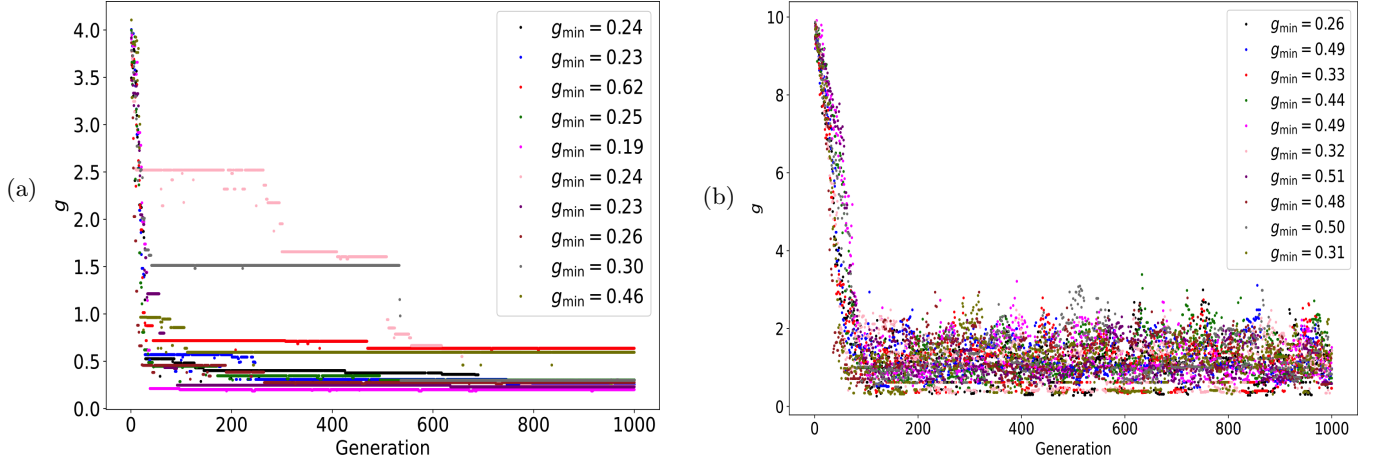


FIG. 23. Different runs of the genetic algorithm. Each color depicts a run with a randomly chosen initial population for $\gamma = 0.31$ and $(J_1, J_2, J_3, J_4) = (3, 4, 1, 2)$ for different system sizes: (a) $N_x = N_y = 4$, population size 100. (b) $N_x = N_y = 6$, population size 100. In these plots, g_{\min} refers to the minimum value of the gap encountered in the run.

Increasing the population size, letting the simulation run for a larger number of generations, *etc.* can be used to reduce the spread of data over different runs.

Appendix C: Some Flux Configurations from the Genetic Algorithm

Here we list some flux configurations for first decay modes obtained from the genetic algorithm. Relative to the NESS where all the gauge-invariant \mathbb{Z}_2 data are set to -1 , we list all the $+1$ defects (*i.e.* plaquette fluxes and Wilson phases). As noted in the text, it may be that each of the states listed here may be describable as having fewer defects with respect to others among the exponentially many (2^{3N+1}) states in the NESS block.

For $N_x = N_y = 4$, $J_1 = J_2 = J_3 = J_4 = 1$:

- $\gamma < 0.41$: $\Phi_{1,1}^+$, $\Phi_{4,2}^-$, $\Phi_{1,3}^-$, $\Phi_{4,2}^+$, $\Phi_{2,4}^-$, $\Phi_{3,3}^+$, $\Phi_{2,4}^+$, $\Phi_{3,1}^-$, $\Omega_{1,1}^+$, $\Omega_{1,3}^-$, $\Psi_{2,2}^-$, $\Psi_{4,2}^+$, W_x , W_y
- $\gamma = 0.41$: $\Phi_{1,1}^+$, $\Phi_{2,2}^-$, $\Phi_{3,1}^+$, $\Phi_{4,2}^-$, $\Phi_{1,3}^-$, $\Phi_{2,2}^+$, $\Phi_{3,3}^-$, $\Phi_{1,3}^+$, $\Phi_{2,4}^-$, $\Phi_{3,3}^+$, $\Phi_{1,1}^-$, $\Phi_{2,4}^+$, $\Phi_{3,1}^-$, $\Phi_{4,4}^+$, $\Omega_{4,2}^+$

- $\gamma > 0.41$: $\Phi_{1,3}^+, \Phi_{3,3}^+, \Phi_{4,4}^-, \Phi_{2,4}^+, \Phi_{3,1}^-, \Phi_{4,4}^+, \Omega_{4,4}^-$

For $N_x = N_y = 6$, $J_1 = J_2 = J_3 = J_4 = 1$:

- $\gamma < 0.36$: $\Phi_{3,1}^+, \Phi_{1,3}^-, \Phi_{2,2}^+, \Phi_{3,3}^-, \Phi_{5,3}^-, \Phi_{6,2}^+, \Phi_{2,4}^-, \Phi_{3,3}^+, \Phi_{6,4}^-, \Phi_{1,5}^-, \Phi_{3,5}^-, \Phi_{4,4}^+, \Phi_{6,4}^+, \Phi_{2,6}^-, \Phi_{5,5}^+, \Phi_{1,1}^-, \Phi_{5,1}^-, \Phi_{6,6}^+, W_y$
- $0.36 \leq \gamma \leq 0.41$: $\Phi_{3,1}^+, \Phi_{1,3}^-, \Phi_{2,2}^+, \Phi_{1,3}^+, \Phi_{3,3}^+, \Phi_{6,4}^-, \Phi_{4,4}^+, \Phi_{1,5}^+, \Phi_{2,6}^-, \Phi_{4,6}^-, \Phi_{5,5}^+, \Phi_{2,6}^+, \Psi_{2,6}^-, W_x$
- $\gamma > 0.41$: $\Phi_{1,1}^+, \Phi_{2,2}^+, \Phi_{4,2}^+, \Phi_{6,2}^+, \Phi_{1,3}^+, \Phi_{3,3}^+, \Phi_{4,4}^-, \Phi_{6,4}^-, \Phi_{2,4}^+, \Phi_{6,4}^+, \Phi_{2,6}^-, \Phi_{1,1}^-, \Phi_{5,1}^-, \Phi_{6,6}^+, \Omega_{4,2}^+, W_x, W_y$

For $N_x = N_y = 4$, $(J_1, J_2, J_3, J_4) = (3, 4, 1, 2)$:

- $\gamma < 0.86$: $\Phi_{1,1}^+, \Phi_{2,2}^-, \Phi_{3,1}^+, \Phi_{4,2}^-, \Phi_{1,3}^-, \Phi_{2,2}^+, \Phi_{3,3}^-, \Phi_{4,2}^+, \Phi_{1,3}^+, \Phi_{2,4}^-, \Phi_{4,4}^-, \Phi_{1,1}^-, \Phi_{2,4}^+, \Phi_{4,4}^+, \Psi_{2,4}^-, \Psi_{4,4}^-, W_x$
- $0.86 \leq \gamma \leq 1.06$: $\Phi_{1,1}^+, \Phi_{2,2}^-, \Phi_{4,2}^-, \Phi_{1,3}^-, \Phi_{2,2}^+, \Phi_{4,2}^+, \Phi_{1,3}^+, \Phi_{3,3}^+, \Phi_{4,4}^-, \Phi_{1,1}^-, \Phi_{2,4}^+, \Phi_{4,4}^+, \Psi_{4,4}^-, W_y$
- $\gamma > 1.06$: $\Phi_{4,2}^-, \Phi_{1,3}^-, \Phi_{3,3}^-, \Phi_{4,2}^+, \Phi_{2,4}^-, \Phi_{3,3}^+, \Phi_{4,4}^-, \Phi_{1,1}^-, \Phi_{2,4}^+, \Phi_{4,4}^+, \Psi_{4,2}^-, W_x, W_y$

For $N_x = N_y = 6$, $(J_1, J_2, J_3, J_4) = (3, 4, 1, 2)$:

- $\gamma < 0.16$: $\Phi_{1,1}^+, \Phi_{4,2}^-, \Phi_{5,1}^+, \Phi_{2,2}^+, \Phi_{4,2}^+, \Phi_{6,2}^+, \Phi_{1,3}^+, \Phi_{2,4}^-, \Phi_{3,3}^+, \Phi_{4,4}^-, \Phi_{6,4}^-, \Phi_{1,5}^-, \Phi_{3,5}^-, \Phi_{4,4}^+, \Phi_{5,5}^-, \Phi_{4,6}^-, \Phi_{5,5}^+, \Phi_{6,6}^-, \Phi_{2,6}^+, \Phi_{3,1}^-, \Omega_{3,1}^+, \Omega_{3,1}^-, \Psi_{3,1}^-, \Psi_{3,1}^+$
- $0.16 \leq \gamma \leq 0.51$: $\Phi_{1,1}^+, \Phi_{2,2}^-, \Phi_{3,1}^+, \Phi_{4,2}^+, \Phi_{6,2}^+, \Phi_{1,3}^+, \Phi_{2,4}^-, \Phi_{3,3}^+, \Phi_{4,4}^-, \Phi_{5,3}^+, \Phi_{2,4}^+, \Phi_{3,5}^-, \Phi_{5,5}^-, \Phi_{6,4}^+, \Phi_{2,6}^-, \Phi_{2,6}^+, \Phi_{3,1}^-, \Phi_{4,6}^+, \Psi_{3,3}^-, W_y$
- $\gamma > 0.51$: $\Phi_{1,1}^+, \Phi_{3,1}^+, \Phi_{4,2}^-, \Phi_{5,1}^+, \Phi_{2,2}^+, \Phi_{4,2}^+, \Phi_{5,3}^-, \Phi_{2,4}^-, \Phi_{3,3}^+, \Phi_{5,3}^+, \Phi_{6,4}^-, \Phi_{2,4}^+, \Phi_{1,5}^+, \Phi_{5,5}^+, \Phi_{6,6}^-, \Phi_{3,1}^-, \Phi_{5,1}^-, \Phi_{6,6}^+, \Psi_{1,1}^-, W_x, W_y$